Fine structure of dark and bright excitons in vertical electric fields: Atomistic theory of alloyed self-assembled InGaAs quantum dots

Michał Zieliński *

Institute of Physics, Faculty of Physics, Astronomy and Informatics, Nicolaus Copernicus University, Ulica Grudziadzka 5, 87-100 Toruń, Poland

(Received 10 October 2020; revised 8 December 2020; accepted 9 December 2020; published 22 December 2020)

The vertical electric field response of dark- and bright-excitonic fine structures in self-assembled quantum dots remains largely unexplored. Using an atomistic tight-binding model, combined with a configuration-interaction approach, we show that the fine structure of both bright and dark excitons can be effectively tuned with a vertical field. The dark-exciton splitting reveals parabolic evolution under an applied electric field, contrary to linearlike trends for the bright-exciton splitting, with a linear change rate of the latter related to the bright-dark splitting. Atomistic results are further investigated in terms of the hole-band-mixing term, which reverses its sign under the electric field leading to a vanishing bright-exciton fine structure, and a minimum of the dark-exciton splitting in a nonalloyed case. Surprisingly, we find that the dark-exciton optical activity is also highly tunable with the electric field, despite the quantum dot's cylindrical shape, with potential implications for applications involving dark excitons. Finally, we study different random realizations of the same alloyed quantum dot, showing that mere alloy randomness substantially affects the bright-exciton splitting both at zero field and at the splitting minimum.

DOI: 10.1103/PhysRevB.102.245423

I. INTRODUCTION

The optically active bright-exciton states confined in quantum dots [1,2] are an important platform for various schemes of entanglement generation [3–6], whereas optically inactive (or weakly active) states, known as dark excitons [7], are considered for applications in quantum-information processing [8–13]. The details of bright- and dark-exciton spectra, the excitonic fine structure [7], are strongly determined by quantum-dot morphological properties [14–19], with various growth and postgrowth schemes [20–29] aiming for reduction of the bright-exciton splitting in particular. Moreover, there have been extensive efforts to control the fine-structure splitting with the postgrowth application of external fields [5,30–39]. From a theoretical point of view, detailed modeling of the excitonic fine structure still presents a formidable computational challenge both for approaches utilizing continuum-media approximation [15,40,41] and even for atomistic methods [10,18,42]. In this work we use the tight-binding method coupled with the configuration-interaction (exact diagonalization) approach, which has been proved to be able to report an excitonic fine structure in good agreement with experiment [18,43,44]. We study the properties of bright and dark excitons under the influence of vertical electric field for both an idealized, nonalloyed, self-assembled InAs/GaAs quantum dot of high symmetry and for a more realistic alloyed $In_{0.5}Ga_{0.5}As$ quantum dot of low symmetry. We compare the results of atomistic calculation with a phenomenological model, which allows us to correlate the field-induced evolution of the bright-exciton splitting with the dark-bright-exciton splitting (isotropic exchange interaction). Moreover, we find that the electric field is able to strongly tune the dark-exciton optical activity. This effect occurs in the absence of symmetry-reducing facets [10], or other shape deformation [45], and is merely due to the field along the growth axis.

The paper is organized as follows. After a brief theoretical introduction in Sec. II, we start in Sec. III by inspecting an idealized, lens-shaped InAs quantum dot of C_{2v} symmetry embedded in the GaAs barrier. By discussing its single-particle spectra and in particular changes of charge probability distribution of electron and hole states, we can gain some understanding of how these relate to the details of excitonic spectra. A considerable part of Sec. III aims to bridge an atomistic description of the excitonic fine structure and an effective model given in terms of light-hole/heavy-hole mixing. Section IV provides a thorough discussion of a nonalloyed system giving a foundation for further studies of alloyed quantum dots.

II. SYSTEMS AND METHODS

The calculation starts with finding atomic positions that minimize the total elastic energy, by using the valence force field method of Keating [46,47] and minimization of strain energy performed with the conjugate gradient method [48,49]. Next the piezoelectric potential [50–54] is calculated by accounting for both linear and quadratic contributions, with piezoelectric coefficients from Ref. [52]. The single-particle spectra of electrons and holes are obtained with the empirical $sp^3d^5s^*$ tight-binding method accounting for d orbitals

*mzielin@fizyka.umk.pl

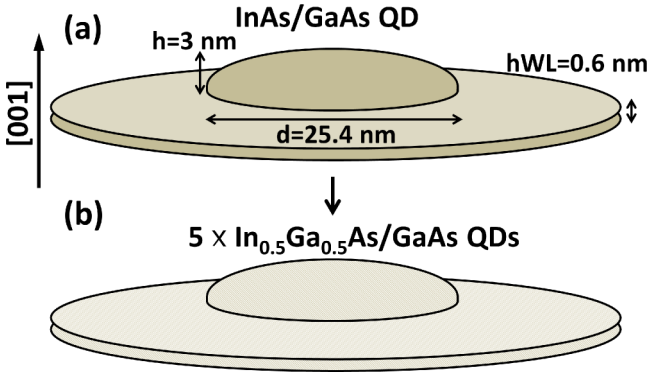

FIG. 1. Schematics of systems under consideration: (a) lens-shaped InAs/GaAs self-assembled quantum dot located on a wetting layer and (b) alloyed $In_{0.5}Ga_{0.5}As$ quantum dots with the same dimensions, however with five randomly generated samples (realizations) corresponding to the same average composition, yet different (random) atomic arrangement. See the text for details. The surrounding GaAs material is not shown.

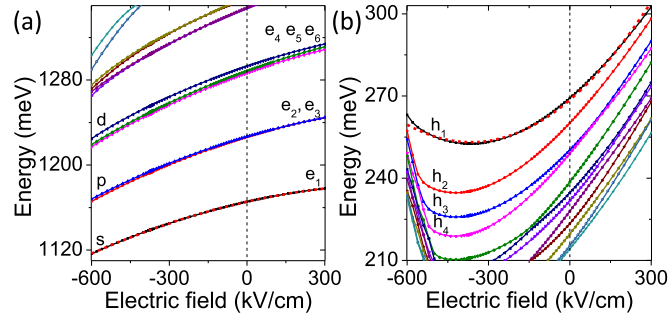

FIG. 2. Single-particle (a) electron and (b) hole spectra of the nonalloyed InAs/GaAs quantum dot as a function of external electric field. Dashed red lines for e_1 and h_1 are fits to a model calculation. Vertical dashed black lines are guides to the eye for zero-field cases. Note the reverse ordering of hole states. See the text for more details.

and spin-orbit interaction [44,55–57]. The tight-binding calculation is effectively performed on a smaller domain than the valence force field calculation [58,59]. The details regarding the $sp^3d^5s^\star$ tight-binding calculations for various nanostructures have been discussed thoroughly in our earlier papers [44,48,57,60]. A static vertical electric field is included in the tight-binding calculation via a potential-energy shift of the orbital energies [61,62] (see the Appendix). Finally, the excitonic spectra [63] are calculated with the configuration-interaction method described in detail in Ref. [60]. More details regarding the Coulomb matrix element computation for tight-binding wave functions can also be found in Refs. [64,65] as well as in our recent papers [66,67].

We start the discussion of the results with the electric field dependence of a C_{2v} nonalloyed InAs/GaAs lens-shaped quantum dot located on a wetting layer [Fig. 1(a)]. The height of the quantum dot is equal to 3 nm and its diameter is 25.4 nm. The quantum dot is located on a 0.6-nm-thick (one lattice constant) wetting layer. Such a quantum-dot system has been studied thoroughly in the literature (including our own work [44,57]) as a model of an idealized self-assembled quantum dot. Here we start by analyzing its general properties, in particular single-particle spectra under an electric field, and later show how these relate to the details of the bright- and dark-exciton many-body spectrum field dependence. In the process, we calculate the spectra of excitons with the full tight-binding/configuration-interaction approach for over 70 different field values. The nonalloyed lens-shaped quantum dot is also used as a convenient starting point to understand the properties of more realistic, alloyed self-assembled quantum dots, which are discussed extensively in Sec. IV. We consider there five random samples [Fig. 1(b)], or five different random realizations of the same alloyed lens-shaped quantum dot, with nominally the same average composition yet different atomic arrangement on a microscopic scale. We consider a 50% admixture of barrier material in the dot region, i.e., an $In_{0.5}Ga_{0.5}As$ quantum dot in the GaAs surroundings, thus with a composition close to experimental systems [7,68–71], with a uniform averaged composition profile, rather than accounting for the effects of spatial changes in the overall composition [70,72–75]. For each quantum-dot realization, the field calculation is performed for at least 40 different field values, altogether (more than 200 cases) presenting a significant computational challenge.

III. NONALLOYED InAs/GaAs QUANTUM DOTS

Let us start by inspecting the evolution of single-particle states under an external electric field as shown in Fig. 2. Electron states demonstrate a well-defined shell structure [1], which remains unaltered even in the presence of the field. They also reveal a mostly quasilinear drift of energies under an applied field, indicating a substantial built-in dipole moment [76] as a result of the quantum dot's lens shape. On the other hand, hole states show the lack of a shell structure for the zero-field case, a well-known effect [44] occurring for strained, lens-shaped InAs/GaAs quantum dots. Moreover, an external field strongly affects the interlevel spacing and splittings of hole states. For example, h_3 and h_4 apparently cross at the field value of approximately 80 kV/cm, whereas h_2 and h_3 do not form a p shell for all fields considered. The field-induced evolution of the hole ground state has a more parabolic dependence displaying a substantial polarizability of the hole states, with an apparent energy minimum of h_1 for a field value equal to -370 kV/cm. These field dependences can be quantified. By treating the external field as a perturbation, the evolution of both electron and hole energies can be fit to a formula [76]

$$E = E_0 + pF + \beta F^2, \tag{1}$$

where p is a built-in dipole moment (linear term), β measures the polarizability (quadratic term), and F is the magnitude of the electric field in the z axis. For the electron and hole ground states Eq. (1) fits very well the atomistic calculation. This fit is shown as thick red dashed lines in Fig. 2. For the electron $p = 5.47 \times 10^{-4}$ kV^{-1} cm and $\beta = -4.45 \times 10^{-6}$ kV^{-2} cm^2. For the hole ground state, we obtain $p = 8.45 \times 10^{-4}$ kV^{-1} cm and $\beta = 11.6 \times 10^{-6}$ kV^{-2} cm^2. Thus, the hole has magnitudes of both linear (dipole moment) and nonlinear (polarization) coefficients approximately twice as

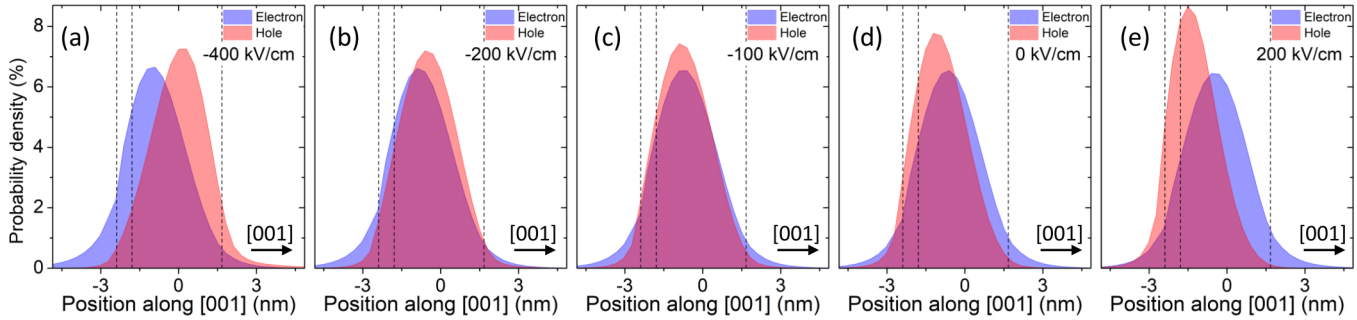

FIG. 3. Single-particle electron and hole ground-state probability densities (integrated over the [100]/[010] plane) for several values of external electric field and as a function of position along the growth [001] axis. Two closely spaced vertical dashed lines mark the position of the wetting layer and the third line corresponds to the top of the quantum dot. The strongest overlap is observed for a field of −100 kV/cm, whereas a nonvanishing dipole moment between the electron and hole can be seen at the zero field. See the text for details.

large as those of the electron, indicating stronger hole-state susceptibility to the external field as also apparent from an inspection of Fig. 2.

A. Single-particle states

The field-related evolution of single-particle energies is accompanied by a change in single-particle charge densities as shown in Figs. 3 and 4, which were obtained by summing the charge probability in the lateral and growth directions, respectively. We note that (for the sake of clarity) Fig. 3 shows charge densities on anion layers only. For comparison, a picture showing charge densities on both anion and cation layers is presented in Appendix A.

Since the electric field has the opposite effect on electron and hole charges, it moves them in opposite directions along the [001] growth axis. For negative-field values the electron charge is pushed toward the bottom of the quantum dot, whereas the hole state is shifted toward its upper part [Fig. 3(a)]. However, already for the zero-field case [Fig. 3(d)], the electron and the hole have maxima of their charge distributions somewhat shifted from each other in the vertical direction, leading to the formation of a built-in dipole moment. This effect has been studied in the literature [77–79] and results from the dome/lens shape of a quantum dot (rather than from a graded composition profile that is not present in C_{2v} quantum dots). As a result of the nonvanishing dipole moment between the electron and hole in the zero field, for (relatively small magnitude) negative-field values the electron and hole states are apparently brought "closer" to each other, whereas for positive-field values the electron and hole are further separated. For a field approximately equal to −100

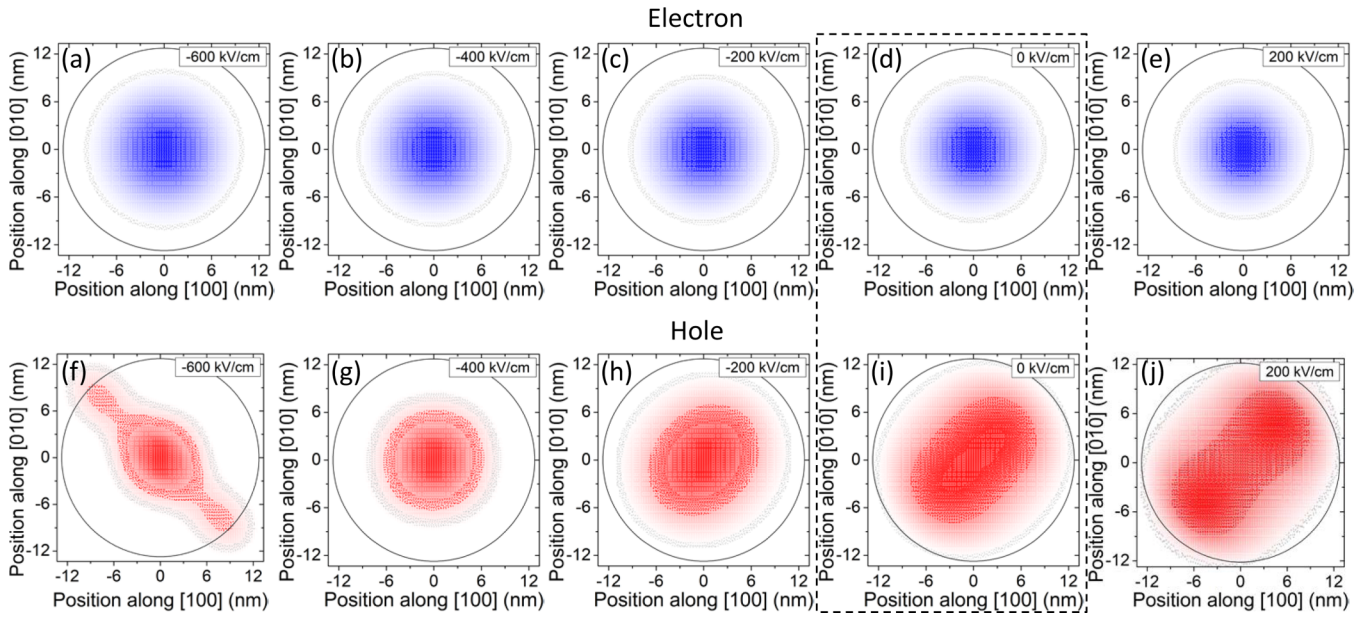

FIG. 4. Single-particle electron and hole ground-state probability densities (integrated along the [001] direction) for several values of the external electric field, as a function of position on the [001]/[010] plane. The dashed box highlights the zero-field case. Whereas the electric field does not alter the lateral probability density of the electron state significantly, it spatially reorients the hole ground state, with its elongation changing from along [110] for positive fields to [1$\bar{1}$0] for negative. At approximately −400 kV/cm the elongation of the hole ground state apparently vanishes, with both the electron and hole having approximate cylindrical symmetry. See the text for more details.

kV/cm [Fig. 3(c)] the overlap of the electron and hole ground states reaches an apparent maximum along the growth axis and is reduced with a further increase of field magnitude [Figs. 3(a) and 3(b)]. Thus, the vertical electric field maximizes the probability density overlap in the growth axis, between electron and hole ground states, for field values close to −100 kV/cm.

In contrast, the spatial overlap viewed in the lateral quantum-dot plane (Fig. 4) reveals a different trend. The lateral charge density distribution of the electron ground state is rather immune to the vertical electric field, with this state retaining its (quasi)cylindrical symmetry over the entire range of field values considered. However, the hole ground state undergoes a rather different and nontrivial field evolution. For the zero field [Fig. 4(i)] the hole ground state is elongated in the [110] direction due to the underlying crystal lattice, the presence of strain, and piezoelectricity. This elongation is further increased for positive-field values, yet it is systematically decreased for negative-field values. For a large magnitude of negative fields [e.g., −600 kV/cm, Fig. 4(f)] the direction of elongation is fully reversed with respect to the zero-field case and the hole ground state is elongated along the $[1\bar{1}0]$ direction. Importantly, for field values close to −400 kV/cm the elongation of the hole ground state vanishes, with both electron and hole ground states having an approximate cylindrical symmetry. This effect is also reflected in the hole-energy spectra [Fig. 2(b)], where the hole ground-state energy reaches its minimum.

The hole ground state is thus subject to lateral elongation in the [110] direction for positive-field values, where part of the hole charge density penetrates the wetting layer. However, the hole ground state gets elongated also along $[1\bar{1}0]$ for the negative-field values, where a substantial part of the hole wave function reaches the curved interface at the top surface of the quantum dot. At approximately −400 kV/cm both contributions apparently compensate each other, leading to a quasicylindrical spatial distribution as shown in [Fig. 4(g)], with notable consequences for the excitonic fine-structure splitting, as discussed further in the text.

B. Bright excitons

Before we inspect the details, let us investigate the main features of excitonic spectra as shown in Fig. 5(a). The lowest excitonic states (the fine structure is not visible on this energy scale) are well separated from the rest of the spectra. Only for the largest field magnitudes considered, higher excitonic states start to coalesce and rapidly decrease toward the lower part of the spectrum. However, in the range of electric field values considered the exciton is still well bound within the quantum dot and its ground state is well separated from the highly excited part of the spectrum. The field-induced evolution of excitonic levels follows a parabolic trend [Fig. 5(a)], as expected from mostly parabolic changes of single-particle levels, which constitute the exciton. The exciton ground-state energy reaches its maximum for a field approximately equal to −70 kV/cm, this maximum being a net effect of single-particle energies and the electron-hole interaction evolution in the field [Fig. 5(b)]. Should we neglect the electron-hole interaction, i.e., assume an excitonic energy equal to the single-particle gap $E_X \approx e_1 - h_1$, the evolution of the exciton ground state would be very similar. In such a case the only notable difference would be the energy maximum shifted to −110 kV/cm, indicating that excitonic field evolution is dominated by the contribution from the single-particle states. Nevertheless, it is still instructive to study further the electron-hole (direct Coulomb) interaction as shown in Fig. 5(b). The ground-state exciton binding energy ΔE_X reaches its minimum for approximately −400 kV/cm. The binding energy is defined as the difference between the exciton ground-state energy E_X and the single-particle effective gap $e_1 - h_1$, indicating the relative strength of the Coulomb interaction, namely,

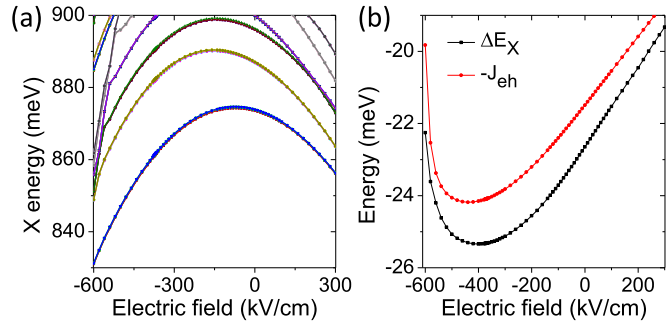

FIG. 5. (a) Several lowest excitonic states and (b) the exciton ground-state binding energy ΔE_X, as well as the electron-hole Coulomb attraction integral $-J_{eh}$ as a function of external electric field for the nonalloyed InAs/GaAs quantum dot. The excitonic binding energy closely follows the Coulomb integral $-J_{eh}$ as apparent from inspection of Eq. (4), with its minimum corresponding to the strongest lateral overlap of electron and hole functions as discussed earlier. See the text for more details.

$$\Delta E_X = E_X - (e_1 - h_1). \tag{2}$$

The trend of excitonic binding energy ΔE_X in Fig. 5(b) is closely followed by the field evolution of the J_{eh} Coulomb integral. This is expected as the exciton ground-state energy can be expressed as

$$E_X = e_1 - h_1 - J_{eh} - \mathrm{corr}(E_X), \tag{3}$$

where J_{eh} is the Coulomb attraction calculated for the electron and the hole in their ground states and $\mathrm{corr}(E_X)$ is the correction due to effects of correlations (in the presence of higher states) and the electron-hole exchange interaction. The above formula leads to

$$\Delta E_X = J_{eh} - \mathrm{corr}(E_X). \tag{4}$$

Since $\mathrm{corr}(E_X)$ usually has values of the order of several meVs, J_{eh} has the dominant contribution to exciton binding energy. Finally, we note that the magnitudes of both ΔE_X and $-J_{eh}$ reach their minima at field values approximately equal to −400 kV/cm, corresponding to the largest electron-hole spatial overlap in the lateral direction, when both the electron and the hole have quasicylindrical symmetry [Figs. 4(b) and 4(g)], rather than for −100 kV/cm, at which the external field maximizes the electron-hole overlap in the growth direction [Fig. 3(c)].

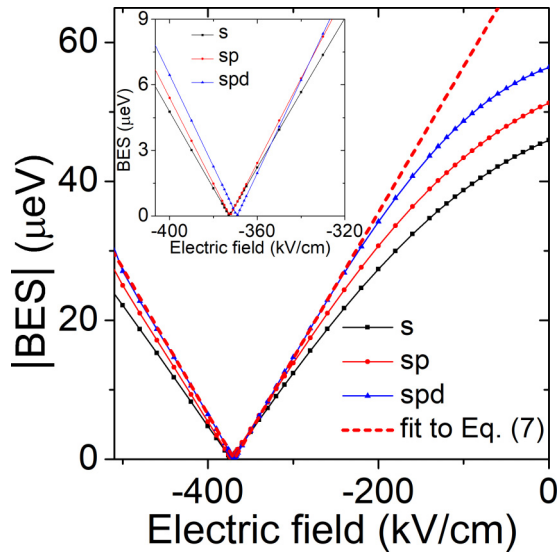

FIG. 6. Absolute value of the bright-exciton splitting as a function of external electric field for different configuration-interaction treatments. Results show different bright-exciton splittings at zero field, yet similar values of the field magnitude corresponding to a vanishing bright-exciton splitting. The red dashed line shows the fit to a phenomenological model. See the text for details.

The evolution of single-particle states has a strong influence on the details of excitonic spectra, namely, the bright-exciton splitting (BES), which is shown in Fig. 6. The BES has a nontrivial field dependence, which is apparently parabolic for small field magnitudes and linearlike for field values lower than approximately −200 kV/cm. At approximately −370 kV/cm the BES goes through zero and the order of the bright-excitonic lines is reversed. Figure 6 also presents the BES at different levels of approximation of the configuration-interaction calculation. Namely, the results are shown for three different configuration-interaction bases involving electron and hole s shells only (four excitonic configurations), with both s and p shells accounted for (36 excitonic configurations), and the most extended calculation with s, p, and d shells included (144 configurations). Since contrary to electrons there is no shell structure of hole levels, these approximations correspond to accounting for the lowest one, three, or six hole states, respectively (or actually two, six, and 12 states with spin; we emphasize again the reverse level ordering for holes). We note that the *spd* treatment is usually sufficient [80] for good quality results of the exciton fine structure in quantum dots, whereas the field calculation with a possibly more accurate approach involving even higher levels is currently beyond our reach due to computational limitations.

Figure 6 shows that the only qualitative difference between various configuration-interaction treatments is notable at the zero field, where the BES goes from 46 through 51 and up to 56 μeV with an increasing number of levels accounted for. These differences are rather small, as could be expected from the (approximately) cylindrical symmetry of the lens-shaped quantum-dot base. Thus, the BES is dominated by a contribution from the electron and hole ground states. Moreover, all configuration-interaction approaches report virtually the same field value (approximately −370 kV/cm) for which the BES vanishes, strongly suggesting that the vanishing fine structure is related to electron and hole ground-state properties.

Let us note that the vanishing bright-exciton fine structure at field values close to −400 kV/cm is consistent with a traditional [7,81,82] understanding of fine-structure splitting originating from breaking of rotational symmetry. In our case, the electric field, by tailoring electron and hole wave functions into quasicylindrical shapes [Figs. 4(b) and 4(g)], is apparently able to reduce the fine structure, although we emphasize that such an analogy would be hard to extend to other C_{2v} nanostructures such as square-based pyramidal quantum dots [43].

To get a better understanding, one can aim to define a phenomenological model, describing the BES evolution in a broad range of field values and preferably defined in the minimal excitonic basis of two bright states only. Following Bennett *et al.* [31], the effective bright-exciton Hamiltonian in the vicinity of a level crossing can be given as

$$\mathbf{H} = \mathbf{I}E_{\mathrm{X}} + \begin{bmatrix} 0 & \frac{S}{2} \\ \frac{S}{2} & -\gamma(F - F_0) \end{bmatrix}, \tag{5}$$

where $\mathbf{I}$ is the identity matrix, E_{X} is the exciton ground-state energy, F_0 is the field value at the minimal splitting of the bright-excitonic doublet, F is the electric field, and γ is the difference in field response between bright states. Moreover, $\frac{S}{2}$ is the off-diagonal part of the BES, which cannot be tuned by a vertical electric field. For convenience, we substitute $E_0 = \gamma F_0$, where E_0 is the contribution to the bright-exciton splitting (at zero field) that can be removed by the electric field. In this model the magnitude of the BES is thus given as

$$|\mathrm{BES}| = \sqrt{S^2 + (E_0 - \gamma F)^2}. \tag{6}$$

Equation (6) could also be viewed as a general formula describing splitting of coupled levels close to an anticrossing.

For the C_{2v} case and no alloying S should be equal exactly to zero by symmetry. This allows for a level crossing, rather than anticrossing, when $S \neq 0$. Thus, in the C_{2v} case and close to the crossing the BES magnitude can be very well described as quasilinear

$$|\mathrm{BES}_{C_{2v}}| \approx |E_0 - \gamma F|. \tag{7}$$

In the case considered $\gamma = 0.21\ \mu\mathrm{eV\,kV^{-1}\,cm}$ and $E_0 = 77.54\ \mu$eV (and thus $F_0 = E_0/\gamma = -369.24$ kV/cm) gives a good quality fit as shown with a red dashed line in Fig. 6(b).

To get more detailed insight into the origins of fine-structure splitting, let us recall the widely used exchange Hamiltonian [7,83] expressed in the basis of bright- and dark-exciton states

$$\mathbf{H}_{\mathrm{exch}} = \frac{1}{2}\begin{bmatrix} \delta_{\mathrm{DB}} & \delta_1 e^{-i\Phi_1} & 0 & 0 \\ \delta_1 e^{i\Phi_1} & \delta_{\mathrm{DB}} & 0 & 0 \\ 0 & 0 & -\delta_{\mathrm{DB}} & \delta_2 e^{-i\Phi_2} \\ 0 & 0 & \delta_2 e^{i\Phi_2} & -\delta_{\mathrm{DB}} \end{bmatrix}, \tag{8}$$

where δ_{DB} describes the bright-dark-exciton splitting, i.e., the quartet splitting into bright and dark doublets, δ_1 is responsible for bright doublet splitting, δ_2 refers to dark-exciton splitting, and Φ_1 and Φ_2 are phase factors, with Φ_1 defining the rotation of polarization axes with respect to a given system

of coordinates (e.g., [110] crystal axis, with typically $\Phi_1 = 0$ for C_{2v} systems). Two blocks of zero off-diagonal matrix elements indicate the lack of bright-dark-exciton coupling due to high system symmetry [7,10]. We also emphasize that various authors use different naming, sign, and phase conventions for δ and Φ. Moreover, these parameters can be obtained either by fitting to experimental results [7,10] or extracted from calculation using various approaches [19,81,82,84]. Analytical calculations can also be performed by expressing the exchange Hamiltonian [85] in a basis spanned by bright $|*\rangle\pm\tilde{1}$ and dark $|*\rangle\pm\tilde{2}$ heavy-hole/light-hole mixed states [85–89]

$$|*\rangle\pm\tilde{1} = \sqrt{1-\beta^2}\left|\pm\frac{3}{2},\mp\frac{1}{2}\right\rangle + \beta e^{-i2\Psi}\left|\mp\frac{1}{2},\mp\frac{1}{2}\right\rangle,$$
$$|*\rangle\pm\tilde{2} = \sqrt{1-\beta^2}\left|\pm\frac{3}{2},\pm\frac{1}{2}\right\rangle + \beta e^{-i2\Psi}\left|\pm\frac{1}{2},\mp\frac{1}{2}\right\rangle, \quad (9)$$

where β is a light-hole contribution which is effectively the measure of that mixing and the angle Ψ (mixing phase) determines the angle of rotation of the quantum-dot main anisotropy axis with respect to the crystal axis [110]. With that approach the absolute value of the bright-exciton splitting for C_{2v} (corresponding to $\Psi = 0$) is given as [85]

$$|\mathrm{BES}| = \left|(1-\beta^2)\Delta_\mathrm{H} + \beta^2\Delta_\mathrm{L} + \frac{4\beta}{\sqrt{3}}\sqrt{1-\beta^2}\Delta_\mathrm{ST}\right|, \quad (10)$$

where Δ_HH and Δ_LH are terms related to heavy- and light-hole contributions, respectively, and Δ_ST refers to the bright-dark splitting. This equation can be rearranged as

$$|\mathrm{BES}| = \left|\beta^2\Delta_\mathrm{LH} + \beta\sqrt{1-\beta^2}\frac{4}{\sqrt{3}}\Delta_\mathrm{ST} + \Delta_\mathrm{HH}\right|, \quad (11)$$

where $\Delta_\mathrm{LH} = \Delta_\mathrm{L} - \Delta_\mathrm{H}$ is introduced for brevity and it can be treated as a single fitting parameter, with the entire equation viewed as a sum of quadratic, quasilinear, and constant terms. Thus, Δ_HH refers to the magnitude of bright-exciton splitting that is present even with vanishing light-hole content and is present in C_{2v} systems due low atomistic symmetry [15].

Retrieving Δ_ST from an atomistic calculation needs some caution since first we typically perform configuration-interaction calculations in a much larger excitonic basis than that of Eq. (8) or (9) and second Δ_ST is related [85] to δ_DB from Eq. (8) as $\delta_\mathrm{DB} = (1 - \frac{4}{3}\beta^2)\Delta_\mathrm{ST}$. One can aim to obtain an effective δ_DB from atomistic results by calculating the energy difference between centers [90] of bright and dark doublets, respectively, and using it instead of Δ_ST. In our case such an approach is particularly well justified since (as will be shown later) $\beta \ll 1$ and thus $\Delta_\mathrm{ST} \approx \delta_\mathrm{DB}$. Therefore, in the following Δ_ST will be replaced with δ_DB. Figure 7 shows both Δ_ST and δ_DB as a function of the electric field and demonstrates that such an approximation is fully justified, with these two quantities practically overlapping on the plot. Figure 7 also shows that the bright-dark splitting changes with the field, with a parabolic dependence with a maximum of 0.38 meV (when accounting for s, p, and d shells) at the field value of approximately -280 kV/cm. We also note that in the range of field values closer to zero (from approximately -100 to 200 kV/cm) the bright-dark-exciton splitting changes quasilinearly with the field. Either way, δ_DB is an apparent function of the electric field [$\delta_\mathrm{DB} \equiv \delta_\mathrm{DB}(F)$]; however, we will continue

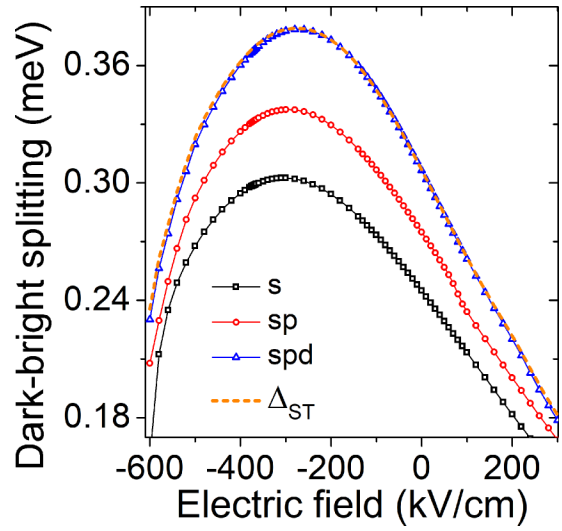

FIG. 7. Bright-dark-exciton splitting as a function of external electric field calculated as the energy difference between the centers of bright-exciton and dark-exciton doublets (δ_DB) at different levels of configuration-interaction treatment. Here $\Delta_\mathrm{ST} = \delta_\mathrm{DB}(1 - \frac{4}{3}\beta^2)^{-1}$ is presented as a dashed line for comparison, showing that $\Delta_\mathrm{ST} \approx \delta_\mathrm{DB}$. See the text for details.

using the simple notation δ_DB for brevity. For comparison, Fig. 7 shows as well the bright-dark-exciton splitting calculated with different configuration-interaction basis sets, all resulting in qualitatively similar results, with the maximum of the isotropic electron-hole exchange interaction close to the field value corresponding to the maximal overlap of electron and hole single-particle wave functions (as shown earlier in Figs. 3 and 4).

Retrieving β from the atomistic calculation is also far from straightforward, due to, e.g., the multiband character of the tight-binding calculation (involving d orbitals), the complicated character of the wave-function envelope with respect to the angular momentum, the presence of multiple excitonic configurations in the configuration-interaction expansion, etc. However, following our earlier work [80,90], one can aim at retrieving the effective value of β from the exciton optical spectra. To this end, Fig. 8(a) shows optical spectra of both bright excitons as a function of the external electric field. Due to the C_{2v} symmetry, excitonic lines are polarized along [110] and [1$\bar{1}$0], with nonzero (approximately 3%) polarization anisotropy in the zero-field case, with polarization anisotropy defined as [87] $C = (I_\mathrm{max} - I_\mathrm{min})/(I_\mathrm{max} + I_\mathrm{min})$.

Both emission lines show a quadraticlike change of intensity under the field, with the maxima of these parabolic dependences being shifted with respect to each other by about 100 kV/cm. Importantly, for the field magnitude of approximately -120 kV/cm both excitons have equal oscillator strength, which leads to a vanishing polarization anisotropy, as confirmed by the inset in Fig. 8(a). Since polarization anisotropy due to hole mixing can be described as [87,88]

$$C(\beta) = \frac{2\beta\sqrt{3(1-\beta^2)}}{3-2\beta^2}, \quad (12)$$

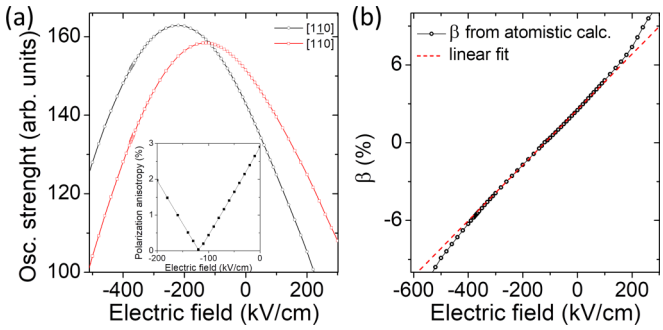

FIG. 8. (a) Bright-exciton oscillator strengths and (b) light-hole β content as a function of external electric field. The inset in (a) shows bright-exciton polarization anisotropy. Nonzero polarization anisotropy at zero field is a hallmark of C_{2v} symmetry and the strong role of the underlying crystal lattice. Vanishing polarization anisotropy at -120 kV/cm corresponds to zeroing of light-hole content β, whereas β content changes quasilinearly with applied vertical field. See the text for details.

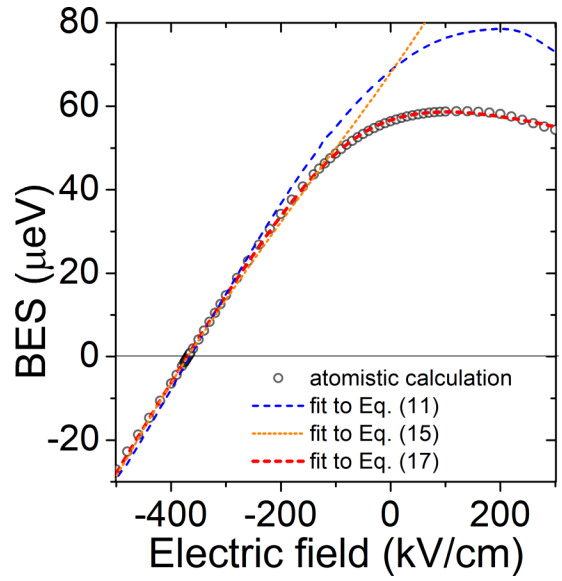

FIG. 9. Bright-exciton splitting as a function of external electric field. Negative values of splitting correspond to reverse order of excitonic lines. Dashed and dotted lines show fits to different models discussed in the text. All models describe very well the linear part of the spectra, close to the anticrossing. However, only an extended model of Eq. (17) is able to provide an accurate description of the splitting close to the zero-field region and for positive-field values. The flat black solid line is a guide to the eye to mark zero splitting.

we can use Eq. (12) to retrieve β from polarization anisotropy calculated atomistically (following Ref. [87] and assuming $\beta > 0$ at zero field); such a β dependence is shown in Fig. 8(b), revealing β to be rather small, i.e., not exceeding 10% in the range of electric field magnitudes studied, and showing a linearlike trend under the electric field in a broad range of values. This trend can be presumed, since for small β values (such as those considered here)

$$C(\beta) \approx \frac{2}{\sqrt{3}}\beta, \tag{13}$$

i.e., polarization anisotropy is proportional to the light-hole content β. Therefore, as a consequence of linearlike change in polarization anisotropy [inset in Fig. 8(a)] under an external field, β demonstrates a linearlike trend as well [Fig. 8(b)]. As a result, the β dependence can be very well fit to a linear function of the field

$$\beta \approx aF + \beta_0, \tag{14}$$

where $a = 0.214\%$ kV^{-1} cm and $\beta_0 = 2.547\%$ is the light-hole content in the zero-field case [Fig. 8(b)], whereas the percentage measure has been used for convenience.

Therefore, the electric field applied in the vertical direction effectively modifies the excitonic light-hole content. At first this may seem surprising; however, since in self-assembled quantum dots strain varies [48,91] substantially along the growth direction (with biaxial strain even changing its sign) and since the biaxial strain is responsible for the light-hole/heavy-hole coupling [92,93], moving or transferring the hole wave function with the electric field (as seen earlier in Fig. 3) from the top to the bottom of a quantum dot (or vice versa), i.e., from regions of opposite signs of biaxial strain, can in turn reverse the sign of β and in effect lead to β reaching zero for a field magnitude of approximately -120 kV/cm. Vanishing β is related to vanishing polarization anisotropy, whereas the actual field value for which this happens will be important for our further investigations of the dark-exciton spectra.

With β and $\Delta_{ST} \approx \delta_{DB}$ retrieved from the atomistic calculation, one can finally use Eq. (11) (i.e., BES $= \beta^2\Delta_{LH} + \beta\sqrt{1-\beta^2}\frac{4}{\sqrt{3}}\delta_{DB} + \Delta_{HH}$), discussed earlier in the text, and fit it to the BES dependence as shown in Fig. 9. With $\Delta_{LH} = 2$ meV, $\Delta_{HH} = 52$ μeV, and both $\beta \equiv \beta(F)$ and $\delta_{DB} \equiv \delta_{DB}(F)$ being functions of the electric field and taken from the atomistic calculation as described above, we obtain a very good fit (Fig. 9), especially in the linear range close to the crossing. However, notably we get only qualitative agreement in the range of positive-field magnitudes. Finally, we note that in Fig. 9 we have additionally omitted the absolute value to empathize the change of BES sign.

Next we note that for small β one can neglect quadratic terms in Eq. (11) and obtain

$$|\mathrm{BES}| \approx \left|\frac{4\beta}{\sqrt{3}}\delta^0_{DB} + \Delta_{HH}\right|. \tag{15}$$

We have further simplified Eq. (11) by assuming that δ^0_{DB} is an effective constant, rather than a function of electric field, and δ^0_{DB} would be estimated at a field range close to the level crossing, rather than at zero field. With $\delta^0_{DB} = 366.8$ μeV and $\delta_{HH} = 46.7$ μeV, we obtain an excellent fit in the region where the bright-exciton splitting vanishes (Fig. 9) and the δ^0_{DB} value is (close to the bright-dark-exciton splitting maximum of 380 μeV) in fact consistent with the initial assumption. We also note that with the help of Eq. (13) one obtains $|\mathrm{BES}| \approx |2C(\beta)\delta^0_{DB} + \Delta_{HH}|$.

Since β is quasilinear with the field, Eq. (15) is equivalent to the previously discussed equation (7) based on Ref. [31]. To bridge these relations, Eq. (15), with the help of Eq. (14),

can be further analyzed in terms of the field dependence, and by comparing Eq. (15) with Eq. (7) we obtain

$$\gamma \propto \delta_{\mathrm{DB}}; \tag{16}$$

thus with the help of the combined atomistic calculation and the phenomenological model, the difference between dipole moments of the two exciton eigenstates γ [31], or the slope of electric field evolution, can be related to the bright-dark splitting (or electron-hole isotropic exchange), which is not only useful for fitting, but also is in itself an interesting theoretical outcome.

Extended phenomenological model

For a C_{2v} quantum dot, with substantial bright-exciton splitting at zero field, Eq. (6) and its linear simplification (7), based on the phenomenological model of Bennet *et al.* as well as our linear formula (15), are apparently unable to reproduce the splitting evolution in the region of small field magnitudes or increasing positive fields (Fig. 9). Equation (11), with quadratic terms in β, is able to describe the trend for positive fields qualitatively (Fig. 9), yet it is impossible to fit Eq. (11) to accurately reproduce the evolution of the bright-exciton splitting at the same time for both the zero crossing and positive-field magnitudes.

To achieve such a desired formula let us return to the model of Ref. [31] and reiterate that at zero field the BES is equal to E_0. This effect is due to the presence of the underlying crystal lattice and the overall C_{2v} quantum-dot symmetry. In addition, E_0 could also be viewed as the result of the nonequivalence of the [110] and [1$\bar{1}$0] directions in C_{2v} quantum dots. We could treat that effectively by replacing E_0 with a functional dependence

$$E_0(F) = E_0' - \sqrt{S_{C_{2v}}^2 + (E_{C_{2v}} - \gamma_{C_{2v}} F)^2},$$

where we have reused Eq. (6), the constants $S_{C_{2v}}$, $E_{C_{2v}}$, and $\gamma_{C_{2v}}$ now describe the BES or $E_0(F)$ dependence in the range of small field values, the lattice/shape anisotropy ($S_{C_{2v}}$ and $E_{C_{2v}}$) dominates over the field contribution, and the prime is used to distinguish from E_0 used previously in Eq. (6).

The dependence $E_0(F)$ is now incorporated back in the BES formula, resulting in

$$|\mathrm{BES}_{C_{2v}}| = |E_0' - \gamma' F - \sqrt{S_{C_{2v}}^2 + (E_{C_{2v}} - \gamma_{C_{2v}} F)^2}|. \tag{17}$$

This effective formula fits well the atomistic data in the entire range of field magnitudes considered, which is shown with a thick red dashed line in Fig. 9, with $S_{C_{2v}} = 23.83$ μeV, $E_{C_{2v}} = -9.32$ μeV, $\gamma_{C_{2v}} = 0.136$ $\mu\mathrm{eV\,kV^{-1}\,cm}$, $E_0' = 82.25$ μeV, and $\gamma' = 0.094$ $\mu\mathrm{eV\,kV^{-1}\,cm}$. At zero field, the splitting is dominated by E_0', yet it is reduced significantly by $-\sqrt{S_{C_{2v}}^2 + E_{C_{2v}}^2} = -25.6$ μeV. Moreover, $(E_{C_{2v}} - \gamma_{C_{2v}} F)^2$ vanishes for $F = E_{C_{2v}}/\gamma_{C_{2v}} \approx 6.9$ kV/cm; thus it is indeed related to small positive-field behavior. On the other hand, for large-magnitude (negative) fields (i.e., close to the level crossing), the splitting is quasilinear with respect to the field with $\gamma \approx \gamma' + \gamma_{C_{2v}} = 0.23$ $\mu\mathrm{eV\,kV^{-1}\,cm}$, therefore, as desired, very close to the linear-model value of 0.21 $\mu\mathrm{eV\,kV^{-1}\,cm}$ found earlier.

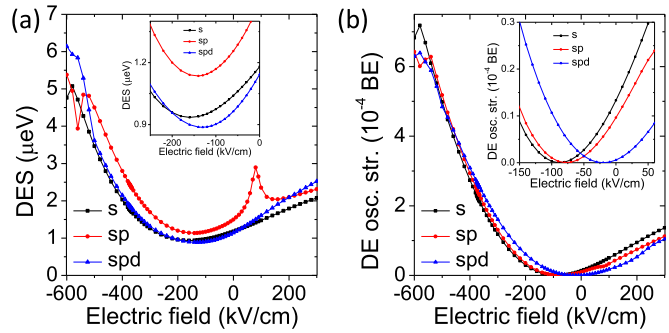

FIG. 10. (a) Dark-exciton splitting and (b) dark-exciton oscillator strengths as a function of external electric field, for different configuration-interaction treatments. Insets show magnifications close to the minima, revealing quadraticlike changes of both dark-exciton splitting and its optical activity in that region. Notably, the dark-exciton splitting minimum does not match the minimum of the z-polarized dark-exciton optical activity. See the text for details.

To summarize, Eq. (17) is able to describe bright-exciton splitting in the broad range of electric values, including the crossing region for a high negative field, and substantial zero-field splitting of the C_{2v} system.

C. Dark excitons

Figure 10(a) shows dark-exciton splitting (DES) calculated as a function of the external electric field for the same C_{2v} lens-shape InAs/GaAs quantum dot studied so far. Consistently with earlier discussion, the results are presented at different levels of configuration-interaction calculation, revealing some interesting differences, yet generally providing good mutual agreement. For field magnitudes close to 80 kV/cm there is an apparent kink in the dark-exciton splitting evolution in the sp approximation, i.e., including the lowest six (12 with spin) electron and hole states (e_1, e_2, e_3 and h_1, h_2, h_3). However, as h_2 and h_3 do not form a shell and h_3 crosses with h_4 at 80 kV/cm, this results in an ill-defined basis for configuration interaction, leading to this artificial feature in the spectra, which naturally vanishes when higher states (incorporating h_4) are accounted for. Apart from that issue, the dark-exciton splitting spectra are very similar in all three bases. As expected [7], the dark-exciton splitting is significantly smaller than the splitting of the bright doublet, with a magnitude of about 1 μeV at zero field. There is also another quite striking difference with respect to the bright exciton, namely, the dark-exciton splitting varies in a quadraticlike manner as a function of the field, especially close to the splitting minimum [inset in Fig. 10(a)]. In the range of electric field magnitudes considered, the dark-exciton splitting changes from approximately 0.9 μeV at the minimum for a field equal to -130 kV/cm up to about 6 μeV for -600 kV/cm. We note that for higher field magnitudes hole states start to rapidly coalesce (eventually leading to breaking of the confined excitonic state), causing irregularities in the dark-exciton splitting plot for large negative fields. Larger field magnitudes are therefore not considered here. Finally, we note that, importantly, the dark-exciton splitting cannot be tuned by the vertical electric field to zero.

The dark-exciton states in C_{2v} systems have nonvanishing optical activity [7,10,15]. Actually, in our case the higher-energy (DE2) dark-exciton state has a weak optical activity with emission polarized along the [001] (z, growth) axis, whereas the lower-energy dark exciton (DE2) remains completely optically inactive. Figure 10(b) shows the DE2 state oscillator strength as a function of the electric field, expressed in units of bright-exciton oscillator strength at zero field. The electric field dependence resembles a parabolic one, especially close to the zero-field region [inset in Fig. 10(b)], with the effect of different shells mostly related to a shift of the field magnitude for which the minimum occurs. In addition, the electric field is able to tune the optical activity of the dark exciton exactly to zero, thus effectively close the radiative decay channel, potentially allowing us to increase the dark-exciton lifetime with possible implications for various quantum-information schemes aiming to utilize dark excitons localized in quantum dots. In contrast, the electric field is also able to substantially increase the optical activity of the dark exciton, which can reach $\frac{1}{20\,000}$ of the one for bright excitons, for large negative fields. Whereas this value appears to be relatively small, the electric field [in the case of the *spd* basis, inset in Fig. 10(a)] effectively increases the dark-exciton oscillator strength by three orders of magnitude as compared to the zero field. Therefore, the electric field can be used in principle to tailor the optical intensity of the dark exciton similarly to shape elongation [19,45,80], shape symmetry breaking [10], and alloying [18]. Nevertheless, it is worth noting that the optical activity of the dark exciton remains rather small compared to that of the bright exciton.

The minimum of the dark-exciton splitting corresponds to nearly the same field magnitude (-130 kV/cm), for which we noticed both polarization anisotropy and β reaching zero. To connect with a phenomenological model and get a better understanding of dark-exciton spectra, one can employ a treatment analogous to that used for the bright exciton, with the exciton basis of heavy-hole/light-hole mixed states [as earlier in Eq. (9)]. For the C_{2v} system this procedure results in a formula for the splitting given in terms of the light-hole content β and δ_{DB} bright-dark splitting, and a parameter δ_2 related to the heavy-hole contribution [85]

$$\mathrm{DES} = (1-\beta^2)\delta_2 + \tfrac{4}{3}\beta^2\delta_{\mathrm{DB}}. \tag{18}$$

Therefore, the dark-exciton splitting is in fact expected to change parabolically as a function of β and as a result (in our case) as a function of the electric field. To study this further, Fig. 11(a) shows again the dark-exciton splitting (in the *spd* configuration-interaction treatment), yet this time compared with the model (18) and terms therein. The only free parameter here is $\delta_2 = 0.885$ μeV, which was chosen to fit the atomistic results. It determines the minimum of the dark-exciton splitting that is due to low C_{2v} symmetry and is mediated by the heavy-hole contribution. Since β^2 is small, $(1-\beta^2)\delta_2 \approx \delta_2$ and this term remains nearly field independent. As the isotropic exchange $\delta_{\mathrm{DB}} \gg \delta_2$, the overall trend is dominated by the quadratic term in β with δ_{DB} acting as a multiplicative factor. However, as $\delta_2 > 0$ the dark-exciton splitting cannot be removed by the electric field, and it is present even if β is tuned to zero. Equation (18) gives thus a solid footing for correlating the vanishing of polarization anisotropy at fields close to -130 kV/cm (and thus β reaching zero) to the minimum in the dark-exciton splitting.

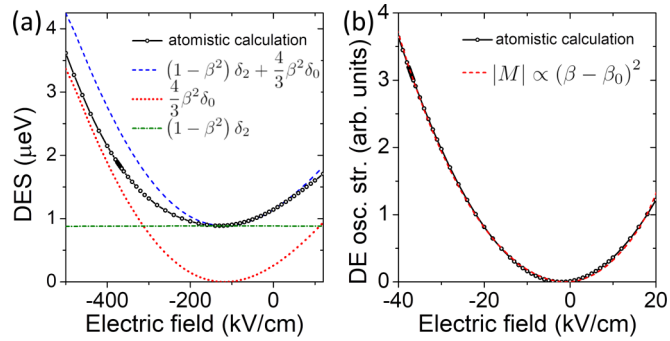

FIG. 11. (a) Dark-exciton splitting as a function of external electric field. The results are the same as the *spd* results shown in Fig. 10(a), but this time compared with the model (18). Terms occurring in Eq. (18) are shown for comparison. (b) Optical activity of the dark exciton as a function of external electric field, with atomistic results [*spd* in Fig. 10(b)] compared now with a phenomenological-model fit showing excellent agreement. See the text for details.

By analyzing Figs. 10(a) and 10(b) one notices that the dark-exciton oscillator strength also change as a quadratic function of the applied field. This is expected, since the dark-exciton optical activity is predicted in a phenomenological modeling to be proportional to the β content [85,86,89]: $|M|^2 \propto \beta^2$. However, in all configuration-interaction treatments considered, the minimum of the dark-exciton optical activity is shifted with respect to the minimum of the dark-exciton splitting ($\beta \approx 0$) by a considerable fraction of the applied field (an approximately -100 kV/cm shift in the *spd* case, corresponding to an approximately 2% difference in β value). To account for this an excellent quality fit to atomistic results can be obtained with

$$|M|^2 \propto (\beta-\beta_0)^2, \tag{19}$$

where $\beta_0 = 2.285\%$ accounts for the shift of the optical activity minimum. There are several possible reasons why β_0 needs to be introduced. One is that the model of Eq. (9) and the formulas it produces (such as $|M|^2 \propto \beta^2$) do not assume any dark-exciton optical activity for a vanishing light-hole content β. This is in contrast to group-theoretic considerations [15] predicting (weak) nonzero optical activity of the dark exciton even for a purely heavy-hole exciton in C_{2v} quantum dots. Therefore, β_0 accounts in part for heavy-hole-related z-polarized optical activity of the dark exciton, which is naturally included in the atomistic treatment. Second, the model (19) is rather simple with β_0 hiding all the complexities, such as changes of the single-particle function shape under the applied field, the complicated multiband character of states, and the many-body treatment.

To summarize, dark-exciton spectra can be tuned with a vertical electric field, revealing parabolic evolution of both dark-exciton splitting and its oscillator strengths, where the latter can be reduced by the field to zero optical activity or conversely increased with the field by a considerable factor. Furthermore, similarly to the bright exciton, a phenomenological model can be used to substantially support the analysis of atomistic results.

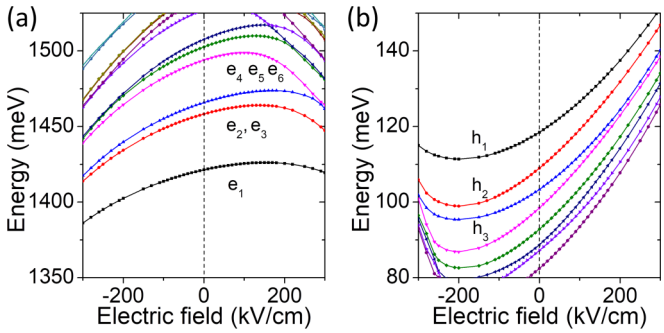

FIG. 12. Single-particle (a) electron and (b) hole spectra of an alloyed $In_{0.5}Ga_{0.5}As$ quantum dot as a function of external electric field. The vertical black dashed line is a guide to the eye for zero-field cases. Note the reverse ordering of hole states. See the text for more details.

IV. ALLOYED InGaAs QUANTUM DOTS

In the following we study the properties of alloyed quantum dots, which could be considered a far better approximation to real self-assembled quantum dots than C_{2v} nonalloyed systems. Alloying has several effects on quantum-dot spectra including the introduction of the high band-gap (GaAs) material into the quantum-dot region that effectively shifts single-particle electron levels higher in energy (by approximately 0.3 eV) [Fig. 12(a)], whereas hole states (due to reversed ordering) are lower in energy (by approximately 0.15 eV) [Fig. 12(b)] than in the nonalloyed case. Alloying will thus increase the difference of single-particle spectra by a considerable value of 350–400 meV. The results presented in Fig. 12 were obtained for one arbitrarily chosen quantum-dot sample, yet results for other samples show similar trends. Further, by mixing with the barrier material, the confining potential depth in the quantum dot is effectively half of that for a nonalloyed quantum dot. As the electron and hole states will reside in a shallower confinement, intershell spacing of electron states will be considerably smaller than in the nonalloyed case, with larger intrashell splittings (e.g., between e_2 and e_3 states). Due to the shallower confinement single-particle states appear to be more strongly affected by the field, and for magnitudes larger than 150 kV/cm (for which e_1 reaches its maximum) higher-lying states start to drift down in energy, effectively breaking the electron shell structure. In contrast, the hole ground state reaches its minimum for the field value of −200 kV/cm, for which the field can approximately restore the shell structure of hole states. This second effect is rather small; however, we checked that it consistently appears in all random samples considered and therefore is not accidental. We also note that for fields of −200 and 300 kV, respectively, hole levels start to strongly coalesce and drift high in energy. For even larger field magnitudes single-particle states start to strongly leak of out the quantum dot and into the barrier; therefore, in the following we do not study the results for field magnitude larger than |400| kV/cm.

Next we follow with Figs. 13 and 14, which show the single-particle probability distribution as a function of electric field, this time for an alloyed system. Figure 13 demonstrates that electron and hole maxima lie at approximately the same spatial position as in the zero-field case. This is a result of the uniform composition profile [78,79] and the fact that alloying significantly reduces spatial anisotropy that dominates the properties of C_{2v} quantum dots and shifts electron and hole positions vertically with respect to each other [as shown earlier in Fig. 3(d)]. The electron ground state is however more spatially delocalized, with larger tails in the barrier and notably smaller probability density at the maximum as compared to the hole. The effect of the field can be mostly described as leading to the separation of electron and hole states. There is also a subtle increase of probability maxima whenever the charge densities are shifted toward the wetting layer, i.e., the lower part of the dot, which is wider in the lateral direction, thus leading to a better spatial localization of single-particle states.

Figure 14 offers the top view of the charge density integrated in the growth direction, revealing rather weak changes of charge distribution in the lateral plane, as an effect of the vertical electric field. Electron states demonstrate very weak elongation along the [110] direction and a rather regular shape despite alloying, whereas the hole ground state shows weak elongation along the $[1\bar{1}0]$ direction, with substantial irregularities due to alloy randomness [94]. Negative fields lead to somewhat large spatial localization of the hole ground states, as the hole state is moved toward the curved top of the quantum dot. Similarly, for positive fields the hole state appears to be spatially more extended, as the hole drifts in the spatially larger wetting layer region. However, in contrast

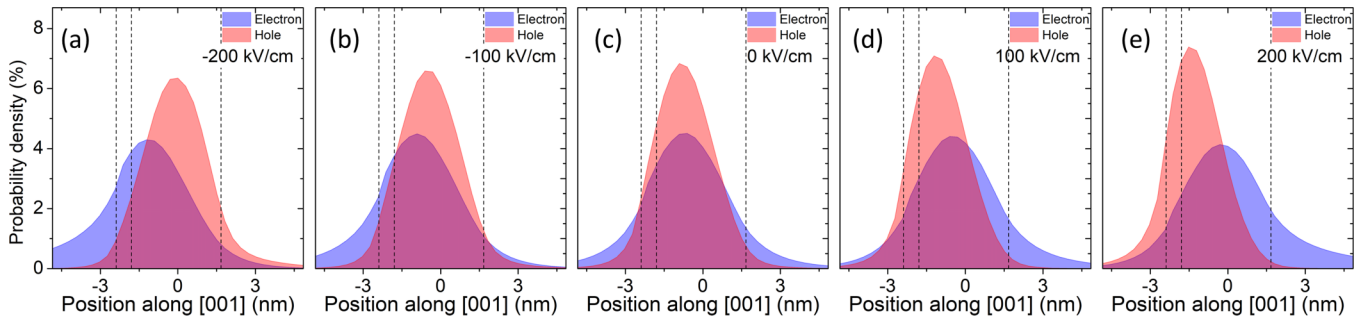

FIG. 13. Single-particle electron and hole ground-state probability density (integrated in the [100]/[010] plane) for an alloyed $In_{0.5}Ga_{0.5}As$ quantum dot and several values of the external electric field, as a function of position along the growth ([001]) axis. Contrary to a C_{2v} quantum dot, there is no apparent dipole moment between the electron and hole at zero field. See the text for details.

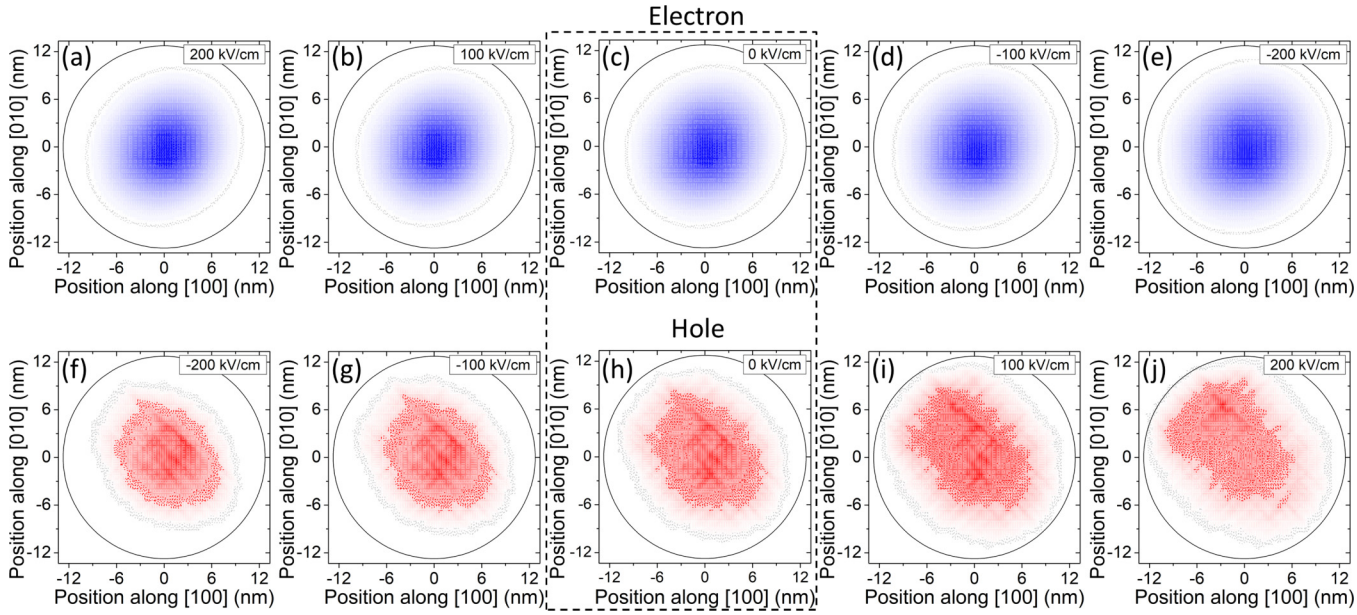

FIG. 14. Single-particle electron and hole ground-state probability density (integrated along the [001] direction) for an alloyed $In_{0.5}Ga_{0.5}As$ quantum dot and several values of the external electric field, as a function of position on the [001]/[010] plane. The dashed box highlights the zero-field case. In contrast to the unalloyed C_{2v} quantum dot, the hole ground state shows only weak elongation along the $[1\bar{1}0]$ direction, with substantial irregularities due to alloy randomness. See the text for details.

to the C_{2v} case, the hole ground state does not undergo an obvious change of spatial orientation with the applied field.

Next Fig. 15(a) shows the excitonic ground-level evolution as a function of the electric field for five different samples (as discussed in the Introduction) with the same average composition and different (random) atomic arrangement. Excitonic energies are considerably (by approximately 400 meV) shifted higher in energy by alloying, reaching 1280 meV at zero field, thus close to typical results for InGaAs quantum dots [9], although we do not aim to match any particular experimental systems. There is an approximately 7-meV spread of excitonic energies between different samples, due to alloy randomness. Alloying reduces the anisotropy of the system; therefore (contrarily to the nonalloyed system), the maxima of excitonic energies occur close to zero field. This can be related to electron and hole single-particle energies reaching their extrema for (approximately) opposite field values, whereas the electron-hole attraction integral has a much weaker contribution, reaching at most 22 meV [inset in Fig. 15(a)], at field values close to -100 kV/cm.

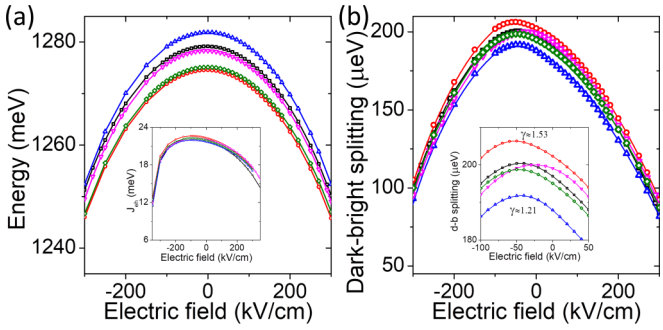

FIG. 15. (a) Several lowest excitonic states and (b) the bright-dark-exciton splitting as a function of external electric field for five alloyed $In_{0.5}Ga_{0.5}As$ quantum dots with the same average composition and different atomic arrangement. The inset in (a) presents changes of the electron-hole attraction integral and the inset in (b) shows magnification of bright-dark splitting close to the maximum. See the text for details.

For larger field magnitudes (both negative and positive) the electric field starts to separate spatially the electron and the hole, reducing the J_{eh} Coulomb interaction. A similar trend can be observed for the bright-dark-exciton splitting calculated for the same group of five quantum dots as a function of the field, shown in Fig. 15(b). With one exception, the maximum of the bright-dark splitting is observed for small negative fields (approximately -50 kV/cm) with an approximately 15-μeV spread of values due to alloying, compared to the 190–200 μeV magnitude of the splitting in the maximum. As a result of shallower confinement, the bright-dark-exciton splitting is considerably smaller than in the nonalloyed case (where it peaked at 380 meV).

A. Bright excitons

Similar to the bright-dark splitting, the bright-exciton splitting [Fig. 16(a)] is also systematically smaller in alloyed systems, with magnitudes varying from 5 to 15 μeV at zero field. This is consistent with experimental results [22,23,31] and can be expected since the intermixing should generally reduce the anisotropy and thus in turn the bright-exciton splitting. We note here that the configuration mixing in alloyed cases is able to shift the position of minima as well as affect the magnitude of the splitting. Nonetheless, qualitatively the bright-exciton splitting is similar in all configuration-interaction treatments. For the sake of clarify, this comparison is left to Appendix B.

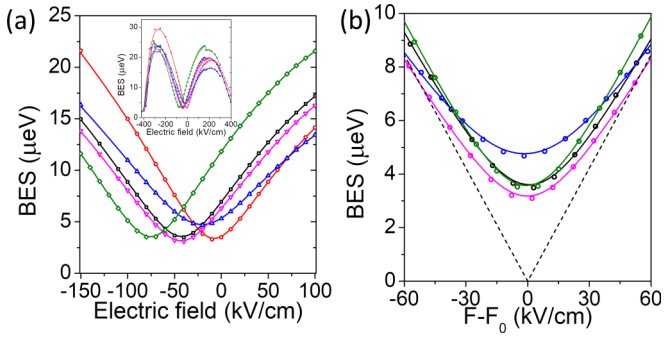

FIG. 16. (a) Bright-exciton splitting as a function of external electric field for five alloyed $In_{0.5}Ga_{0.5}As$ InAs/GaAs quantum dots with the same average composition, yet different atomic arrangement. (b) Same results as in (a) offset by F_0 (i.e., centered at the F_0 field), with one sample omitted for clarity. The black dashed line demonstrates the trend expected for a quantum dot with a vanishing splitting at the crossing for an unalloyed C_{2v} case. For alloyed cases, the splitting cannot be removed by the vertical field only. The inset in (a) shows bright-exciton splitting in a broader range of electric field. See the text for details.

One could expect the bright-exciton splitting to follow the same electric field evolution as the electron-hole direct Coulomb and exchange interactions shown in Fig. 16. Such behavior was found in our recent work [18] for alloyed nanowire quantum dots, where the overall shape symmetry was disklike and the splitting between bright states was simply reduced with the field due to increasing electron-hole separation. However, self-assembled quantum dots have a dome/lens shape, lacking inversion symmetry in the growth direction, leading to a different dipole moment of both bright-exciton species even in an alloyed case. This strongly affects the bright-exciton spectra and leads to an apparent anticrossing of the bright-exciton doublet at relatively small fields. The overall trend of the bright-exciton evolution in alloyed quantum dots is quite complicated; however, close to the minimum it can be very well described by a model of Eq. (6), i.e., $|\mathrm{BES}| = \sqrt{S^2 + (E_0 - \gamma F)^2}$. The position of the anticrossing ($F_0 = E_0/\gamma$) varies from dot to dot (from approximately -10 to -75 kV/cm) and the magnitude of the splitting in the minimum (S) varies from 3 to 5 μeV. We can fit our atomistic result to this equation, with results shown in Fig. 16(b), where for better comparison the results are centered at $F_0 = E_0/\gamma$ and we omitted one sample result for the sake of visual clarity. By fitting we have obtained the set of pairs $S_1 = 3.1$ and $\gamma_1 = 1.28$, $S_2 = 3.3$ and $\gamma_2 = 1.53$, $S_3 = 3.5$ and $\gamma_3 = 1.52$, $S_4 = 3.5$ and $\gamma_4 = 1.41$, and $S_5 = 4.7$ and $\gamma_5 = 1.22$, with S values given in μeV and γ in $\mu\mathrm{eV\,kV^{-1}\,cm}$ and lower indices numbering the samples, which were arbitrarily ordered with an increasing value of S. As noted by Bennet *et al.* [31], there is no apparent correlation between γ and excitonic energy or the splitting magnitude at zero field. However, consistent with our earlier discussion and Eq. (16) (i.e., $\gamma \propto \delta_{\mathrm{DB}}$), we find that there is an apparent correlation between the bright-dark-exciton splitting and γ even in an alloyed case, as illustrated in the inset in Fig. 15(b) with extreme γ values corresponding to extreme values of the bright-dark splitting. We can thus analyze the atomistic results, yet again with the help of a phenomenological approach. For the quantum-dot case with low symmetry the bright-exciton splitting is given as [85]

$$|\mathrm{BES}| = \sqrt{[(1-\beta^2)\Delta_h - \beta^2\Delta_l]^2 + \tfrac{16}{3}(1-\beta^2)^2\beta^2\Delta_{\mathrm{DB}}^2}. \tag{20}$$

Assuming again that β is small in the alloyed case as well and neglecting higher terms in β, we obtain

$$|\mathrm{BES}| \approx \sqrt{\Delta_h^2 + \tfrac{16}{3}\beta^2\Delta_{\mathrm{DB}}^2}; \tag{21}$$

therefore, by assuming a linear change of β with the electric field and comparing Eq. (21) with Eq. (6), we can clearly see that $\Delta_h \approx S$ and $\gamma \propto \Delta_{\mathrm{DB}}$. To further verify how Eq. (21) relates to atomistic results, Figs. 17(a)–17(e) show the bright-exciton optical spectra for five random samples, with insets showing the polarization anisotropy. Since the lattice anisotropy is strongly reduced by alloy randomness, alloyed systems reveal rather weak polarization anisotropy at near-zero fields. With increasing field magnitudes, the overall oscillator strengths are reduced due to increased separation of electron and hole states; however, there are noticeable dips in oscillator strengths in regions corresponding to the bright-exciton splitting minima [Figs. 17(f)–17(j)]. In two cases [Figs. 17(b) and 17(c)] the minima of oscillator strengths of both bright states overlap with each other and the zero of polarization anisotropy matches the minimum of the bright-exciton splitting. In these two particular situations, model predictions match very well atomistic results as shown in Figs. 17(g)–17(j). Here we used β values extracted from the polarization anisotropy case (as we did earlier in the nonalloyed case), Δ_{DB} was also taken from the atomistic calculation, and only a single fitting parameter was used by setting Δ_h equal to S, with S determined earlier in the discussion of Fig. 16. However, in other cases, most notably in Fig. 17(j), there are two apparent dips in polarization anisotropy. One of the dips is related to the bright-exciton splitting minimum occurring at the anticrossing of exciton levels and the second one matches the field region where both bright excitons have the same oscillator strengths (vanishing polarization anisotropy) despite nonzero splitting. Despite these differences, in all cases considered Δ_{DB} very well determines the slope γ of bright-exciton splitting evolution under the electric field.

B. Dark excitons

As the bright-exciton splitting is strongly affected by the electric field, so is the dark-exciton splitting as shown in Fig. 18(a). The evolution of dark-exciton splitting under the electric field resembles parabolic trends observed earlier for the nonalloyed system. The evolution is however generally more complicated in the alloyed system. We found that this is related to an increased role of configuration mixing with higher shells (see Appendix B). Interestingly, the lack of quantum-dot shape inversion symmetry (due to its lens shape and the presence of the wetting latter) has also a pronounced effect on the dark-exciton spectra, which appear to be asymmetric in the field, especially when considering large

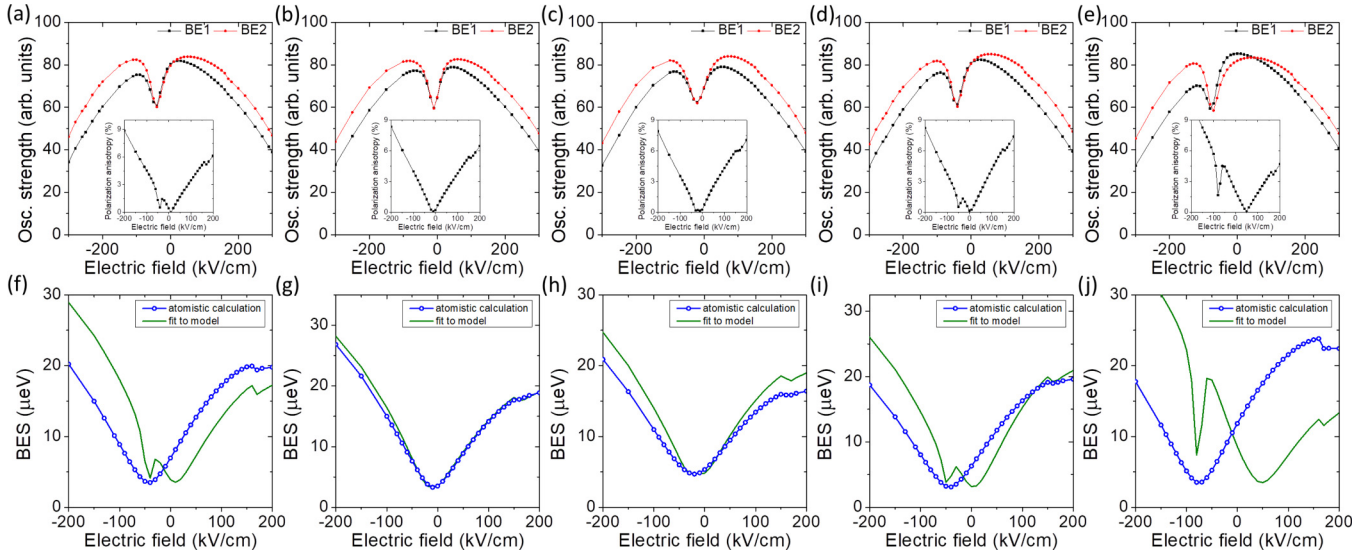

FIG. 17. (a)–(e) Bright-exciton (BE1 and BE2) oscillator strengths as a function of external electric field for five alloyed $In_{0.5}Ga_{0.5}As$ InAs/GaAs quantum dots with the same average composition, yet different atomic arrangement. Insets in (a)–(e) show polarization anisotropy. (f)–(j) Corresponding bright-exciton splitting field evolution, where atomistic results (as presented earlier in Fig. 16) are now compared with a phenomenological model. See the text for details.

field magnitudes. Namely, for large positive fields, the hole state leaking into the wetting layer, and the electron leaking out of the dot [Fig. 13(e)], the magnitude of the splitting reaches approximately 2 μeV, whereas in the opposite case of strong negative fields, the electron leaking into the wetting layer, and the hole leaking toward the (curved) top of the quantum dot, the dark-exciton splitting can reach up to 4 μeV. Notably, in all cases considered the magnitude of the splitting never drops below 1 μeV, except for very large field magnitudes (greater than 400 kV/cm) that effectively push the electron and the hole apart and out of the quantum dot.

As in the C_{2v} case, the position of the dark-exciton splitting minima in alloyed systems is not straightforwardly related to its optical activity minima shown in Fig. 18(b). Importantly, Fig. 18(b) shows also that the effect of strong optical activity enhancement due to a vertical field is present in alloyed C_1 quantum dots as well, having again a well-defined parabolic dependence. In the alloyed case, contrary to the C_{2v} system, both dark excitons can have (weak) nonzero optical activity already at zero field due to low symmetry [15]. Moreover, this activity is not limited to z polarization only, but there are weak oscillator strengths related to the in-plane emission as well. However, only the z-polarized emission of the higher-energy state (DE2) is significantly increased by the electric field. Therefore, in Fig. 18(b) only the z-polarized emission from DE2 is shown; the study of other (small) components is left for future work. Moreover, to compare the different alloyed cases Fig. 18(b) uses the same (arbitrary) units as in Fig. 17 for the bright exciton. Therefore, the dark-exciton emission can reach up to $\frac{1}{1000}$ of the bright-exciton intensity. Figure 18(b) demonstrates again an important possibility of a significant increase of the dark exciton's optical activity with vertical electric fields even in more realistic, alloyed quantum dots. Moreover, even in an alloyed system the z-polarized component of the oscillator strength can be effectively tuned to zero by the field.

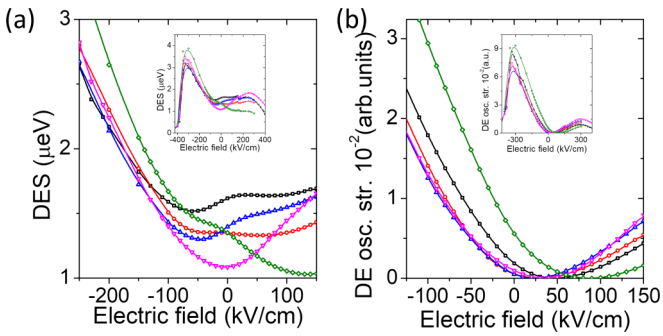

FIG. 18. (a) Dark-exciton splitting and (b) dark-exciton oscillator strength in the [001] (z, growth) direction as a function of external electric field for five alloyed $In_{0.5}Ga_{0.5}As$ InAs/GaAs quantum dots with the same average composition, yet different atomic arrangement. Despite alloying, the vertical electric field can strongly tune z-polarized dark-exciton emission to zero or conversely strongly increase it. Insets show the results in a broader range of electric field. See the text for details.

V. CONCLUSION

We used the tight-binding/configuration-interaction simulations to explore the effects of a vertical electric field on the fine structure of bright and dark excitons in alloyed self-assembled quantum dots. We started with a nonalloyed InAs lens-shaped quantum-dot system, in an attempt to bridge atomistic results and a phenomenological model describing the exciton fine structure in terms of hole-band mixing. We found that the light-hole contribution is effectively tuned by a vertical electric field and as a result so is the exciton fine

structure. We also found that the linear rate at which the bright-exciton splitting changes in the electric field is related to the isotropic electron-hole exchange.

We then followed with a study of an alloyed quantum dot. Instead of calculations with various quantum-dot dimensions or composition profiles, we focused on the role of alloy randomness. We therefore studied five random realizations (samples) of the $In_{0.5}Ga_{0.5}As$ quantum dot with the same dimensions and average composition. We assumed no lateral shape elongation of the quantum dot, which is often used to mimic fine-structure splitting in theoretical approaches struggling to model the exciton fine structure. As a result, we found that the exciton fine structure depends on the interplay of lattice anisotropy and disorder due to alloy randomness. Although we did not attempt to address any particular experiment (which is often very difficult due to experimental uncertainties in sizes, shapes, and compositions [95,96]), our findings are in good agreement with experimental results, in terms of both bright-exciton splitting magnitudes and the corresponding electric field ranges [31,97]. We showed that both bright- and dark-exciton splittings in an alloyed system cannot be tuned to zero by a vertical electric field. In contrast, the optical activity of the dark exciton can be very efficiently controlled with the field, substantially increased or decreased to zero, with possible implications for utilization of dark excitons in quantum-information processing.

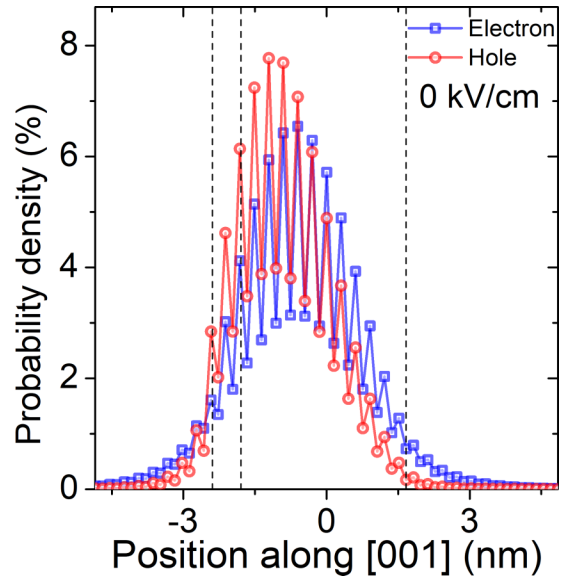

FIG. 19. Single-particle electron and hole ground-state probability density (integrated in the [100]/[010] plane) at zero electric field, as a function of position along the growth ([001]) axis, as in Fig. 3(d) yet with both cation and anion planes accounted for in the plot, showing strongly oscillatory character between nearby anion/cation monolayers. See the text for details.

ACKNOWLEDGMENTS

The author acknowledges support from the Polish National Science Centre based on Decision No. 2018/31/B/ST3/01415. The author would like to thank MichałGawłeczyk for reviewing the manuscript and valuable comments. Further requests regarding technical details of this study can be made to the author.

APPENDIX A: CHARGE DENSITIES ON IONIC PLANES

For the sake of clarity, the charge densities shown in Figs. 3 and 13 were presented on subsequent anion (arsenic) planes only, corresponding to a spatial resolution equal to half of the lattice constant. For comparison, Fig. 19 shows electron and hole probability densities for a nonalloyed quantum dot [at zero field, corresponding to Fig. 3(d)], yet with both cation and anion planes included in the plot. This plot has a quarter of the lattice constant effective spatial resolution and reveals the highly oscillatory atomistic character of single-particle wave functions.

APPENDIX B: CONFIGURATION INTERACTION AND ALLOYING

In Figs. 20(a)–20(e) we show the bright-exciton splitting as a function of vertical electric field, calculated for five random samples and for three different configuration-interaction treatments. The presence of higher shells systematically increases (by up to several μeV) the magnitude of the bright-exciton splitting, both at zero field and at the splitting minimum. The inclusion of higher shells also tends to shift [with the exception of one sample in Fig. 17(c)] the position of the minimum toward a larger magnitude of negative fields. Apart from that, the bright-exciton splitting evolution appears to be qualitatively similar in all treatments, although qualitative difference are not negligible.

Figures 20(f)–20(j) show an analogous comparison for the dark-exciton splitting. For a large magnitude of the negative field ($F < 100$ kV/cm) higher shells (in particular, the p shell) are responsible for a small increase of the dark-exciton splitting, i.e., by a fraction of μeV only. Somewhat larger shifts are observed at zero and positive fields. The differences between all approaches are however small and do not exceed 1 μeV, yet since the dark-exciton splitting is generally relatively small (as compared to the bright-exciton splitting), the configuration mixing apparently affects notably the dark-exciton splitting evolution. In effect, the trend changes from a parabolic to a somewhat more "flat" dependence for positive-field values. Importantly, however, in all cases considered the field is unable to reduce the magnitude of the dark-exciton splitting to zero, as discussed in the main text.

APPENDIX C: ATOMISTIC TIGHT-BINDING CALCULATION

The atomistic tight-binding method (combined with the configuration-interaction approach) we used was described in detail in our earlier works [44,48,57,60,98,99]; here we briefly discuss the main points of the tight-binding method and inclusion of the electric field. The single-particle tight-binding Hamiltonian for the system of N atoms and m orbitals per

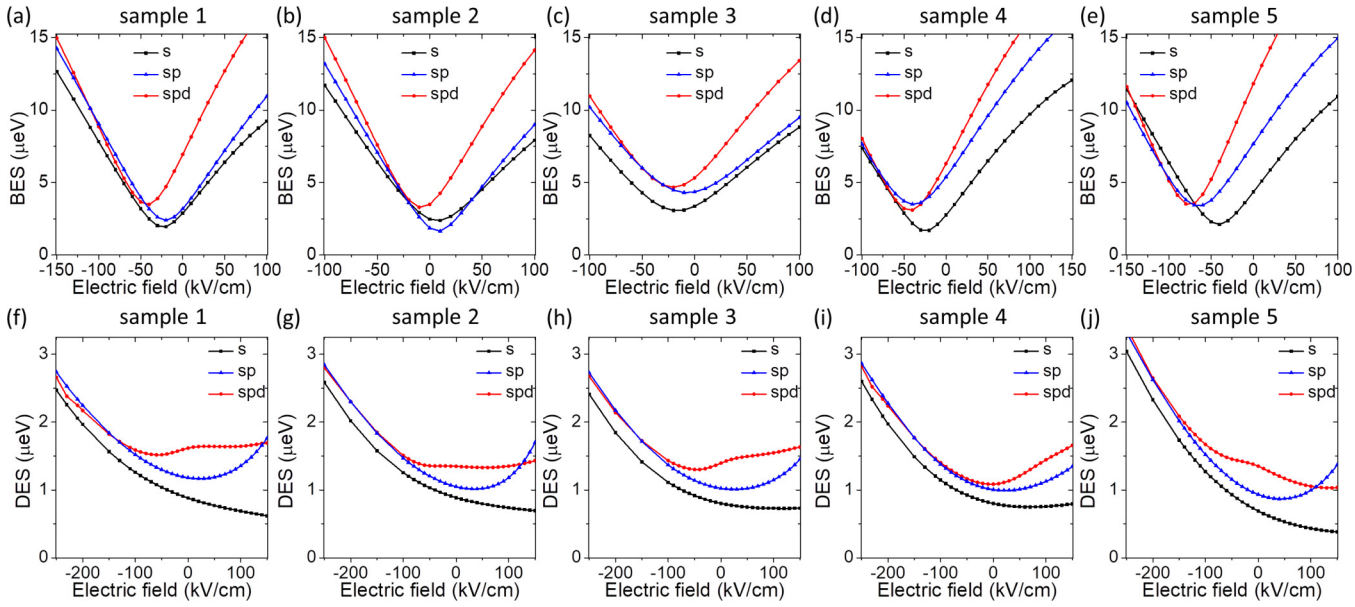

FIG. 20. (a)–(e) Bright-exciton and (f)–(j) dark-exciton splitting calculated at different levels of configuration-interaction treatment for five samples, as a function of the electric field.

atom can be written as [60]

$$\hat{H}_{\mathrm{TB}} = \sum_{i=1}^{N}\sum_{\alpha=1}^{m} E_{i\alpha} c_{i\alpha}^{\dagger} c_{i\alpha} + \sum_{i=1}^{N}\sum_{\alpha=1,\beta=1}^{m} \lambda_{i\alpha,\beta} c_{i\alpha}^{\dagger} c_{i\beta} + \sum_{i=1}^{N}\sum_{j=1}^{\mathrm{NN}}\sum_{\alpha,\beta=1}^{m} t_{i\alpha,j\beta} c_{i\alpha}^{\dagger} c_{j\beta}, \tag{C1}$$

where $c_{i\alpha}^{\dagger}$ ($c_{i\alpha}$) is the creation (annihilation) operator of a carrier on the (spin) orbital α localized on the site i, $E_{i\alpha}$ is the corresponding on-site energy, and $t_{i\alpha,j\beta}$ describes the hopping between the orbitals on the four nearest-neighbor sites. Site i goes over all atoms, whereas j iterates over the four nearest neighbors only. Orbital α is a composite (spin and orbital) index of the on-site orbital, whereas β is a composite index of the neighboring atom orbital. Here $\lambda_{i\alpha,\beta}$ accounts for the spin-orbit interaction following the description given by Chadi [56], using the $sp^3d^5s^*$ parametrization of Jancu *et al.* [55].

In order to account for the external electric field, the electric field potential $\hat{V}$ is added to the tight-binding Hamiltonian as

$$\hat{H} = \hat{H}^0 + \hat{V}, \tag{C2}$$

where $\hat{H}^0$ is zero-field tight-binding Hamiltonian and $\hat{V} \equiv V(\vec{R})$ is the (diagonal) electric field potential calculated at each atomic site $\vec{R}$, which for a static, uniform vertical electric field gives [76] $V(\vec{R}) = eFz$, where e is elementary charge, F is the external electric field (magnitude) applied along the z (growth) direction, and z is the z component of atomic position $\vec{R}$, with $z = 0$ taken at the center of the quantum dot height. Thus we assume that $\hat{V}$ modifies the on-site diagonal matrix elements only [62,100,101], reconciling the accuracy to the necessity of the gauge/choice of the origin invariance [102,103].

Finally, we note that the tight-binding calculation is performed on a smaller domain than strain (valence force field) calculation [58,59], with boundary conditions treated as described in Ref. [58], and the buffer thickness, i.e., the thickness of the GaAs material surrounding both InAs quantum dots (in other words, the separation of InAs quantum dots from the computational box boundary), exceeding 5 nm, thus sufficient to obtain electron and hole spectra with sub-meV accuracy [58,59]. Nonetheless, the computational box still contains 0.6×10^6 atoms and the size of the tight-binding domain exceeds 10×10^7. Since in our numerical tests we found that the perturbative approach [61,104] often fails for larger fields and alloyed systems, the tight-binding Hamiltonian needs to be solved for every field value (followed by a configuration-interaction calculation), thus presenting a formidable computational challenge.

[1] L. Jacak, P. Hawrylak, and A. Wojs, *Quantum Dots* (Springer, Berlin, 1998).

[2] D. Bimberg, M. Grundmann, and N. N. Ledentsov, *Quantum Dot Heterostructures* (Wiley, Chichester, 1999).

[3] *Quantum Dots for Quantum Information Technologies*, edited by P. Michler, Nano-Optics and Nanophotonics Vol. 237 (Springer, Cham, 2017).

[4] O. Benson, C. Santori, M. Pelton, and Y. Yamamoto, Regulated and Entangled Photons from a Single Quantum Dot, Phys. Rev. Lett. **84**, 2513 (2000).

[5] R. M. Stevenson, R. J. Young, P. Atkinson, K. Cooper, D. A. Ritchie, and A. J. Shields, A semiconductor source of triggered entangled photon pairs, Nature (London) **439**, 179 (2006).

[6] M. Prilmüller, T. Huber, M. Müller, P. Michler, G. Weihs, and A. Predojević, Hyperentanglement of Photons Emitted by a Quantum Dot, Phys. Rev. Lett. **121**, 110503 (2018).

[7] M. Bayer, G. Ortner, O. Stern, A. Kuther, A. A. Gorbunov, A. Forchel, P. Hawrylak, S. Fafard, K. Hinzer, T. L. Reinecke, S. N. Walck, J. P. Reithmaier, F. Klopf, and F. Schäfer, Fine structure of neutral and charged excitons in self-assembled In(Ga)As/(Al)GaAs quantum dots, Phys. Rev. B **65**, 195315 (2002).

[8] I. Schwartz, D. Cogan, E. R. Schmidgall, L. Gantz, Y. Don, M. Zieliński, and D. Gershoni, Deterministic coherent writing of a long-lived semiconductor spin qubit using one ultrafast optical pulse, Phys. Rev. B **92**, 201201(R) (2015).

[9] I. Schwartz, E. R. Schmidgall, L. Gantz, D. Cogan, E. Bordo, Y. Don, M. Zielinski, and D. Gershoni, Deterministic Writing and Control of the Dark Exciton Spin Using Single Short Optical Pulses, Phys. Rev. X **5**, 011009 (2015).

[10] M. Zieliński, Y. Don, and D. Gershoni, Atomistic theory of dark excitons in self-assembled quantum dots of reduced symmetry, Phys. Rev. B **91**, 085403 (2015).

[11] J. McFarlane, P. A. Dalgarno, B. D. Gerardot, R. H. Hadfield, R. J. Warburton, K. Karrai, A. Badolato, and P. M. Petroff, Gigahertz bandwidth electrical control over a dark exciton-based memory bit in a single quantum dot, Appl. Phys. Lett. **94**, 093113 (2009).

[12] X. Xu, B. Sun, P. R. Berman, D. G. Steel, A. S. Bracker, D. Gammon, and L. Sham, Coherent population trapping of an electron spin in a single negatively charged quantum dot, Nat. Phys. **4**, 692 (2008).

[13] R. Ohta, H. Okamoto, T. Tawara, H. Gotoh, and H. Yamaguchi, Dynamic Control of the Coupling between Dark and Bright Excitons with Vibrational Strain, Phys. Rev. Lett. **120**, 267401 (2018).

[14] G. Bester, S. Nair, and A. Zunger, Pseudopotential calculation of the excitonic fine structure of million-atom self-assembled $In_{1-x}Ga_xAs$/GaAs quantum dots, Phys. Rev. B **67**, 161306(R) (2003).

[15] K. F. Karlsson, M. A. Dupertuis, D. Y. Oberli, E. Pelucchi, A. Rudra, P. O. Holtz, and E. Kapon, Fine structure of exciton complexes in high-symmetry quantum dots: Effects of symmetry breaking and symmetry elevation, Phys. Rev. B **81**, 161307(R) (2010).

[16] R. Singh and G. Bester, Nanowire Quantum Dots as an Ideal Source of Entangled Photon Pairs, Phys. Rev. Lett. **103**, 063601 (2009).

[17] M. A. Dupertuis, K. F. Karlsson, D. Y. Oberli, E. Pelucchi, A. Rudra, P. O. Holtz, and E. Kapon, Symmetries and the Polarized Optical Spectra of Exciton Complexes in Quantum Dots, Phys. Rev. Lett. **107**, 127403 (2011).

[18] M. Zieliński, Spectra of dark and bright excitons in alloyed nanowire quantum dots, Phys. Rev. B **100**, 045309 (2019).

[19] M. Zieliński, Excitonic fine structure of elongated InAs/InP quantum dots, Phys. Rev. B **88**, 155319 (2013).

[20] M. Abbarchi, T. Kuroda, T. Mano, and K. Sakoda, Fine structure splitting reduction in droplet epitaxy GaAs quantum dots grown on (111) a surface, J. Phys.: Conf. Ser. **245**, 012049 (2010).

[21] A. Kors, J. P. Reithmaier, and M. Benyoucef, Telecom wavelength single quantum dots with very small excitonic fine-structure splitting, Appl. Phys. Lett. **112**, 172102 (2018).

[22] R. J. Young, R. M. Stevenson, A. J. Shields, P. Atkinson, K. Cooper, D. A. Ritchie, K. M. Groom, A. I. Tartakovskii, and M. S. Skolnick, Inversion of exciton level splitting in quantum dots, Phys. Rev. B **72**, 113305 (2005).

[23] W. Langbein, P. Borri, U. Woggon, V. Stavarache, D. Reuter, and A. D. Wieck, Control of fine-structure splitting and biexciton binding in $In_xGa_{1-x}As$ quantum dots by annealing, Phys. Rev. B **69**, 161301(R) (2004).

[24] M. T. Bjork, C. Thelander, A. Hansen, L. Jensen, M. Larsson, L. R. Wallenberg, and L. Samuelson, Few-electron quantum dots in nanowires, Nano Lett. **4**, 1621 (2004).

[25] M. T. Borgström, V. Zwiller, E. Müller, and A. Imamoglu, Optically bright quantum dots in single nanowires, Nano Lett. **5**, 1439 (2005).

[26] D. Dalacu, A. Kam, D. G. Austing, X. Wu, J. Lapointe, G. C. Aers, and P. J. Poole, Selective-area vapour-liquid-solid growth of InP nanowires, Nanotechnology **20**, 395602 (2009).

[27] D. Dalacu, K. Mnaymneh, J. Lapointe, X. Wu, P. J. Poole, G. Bulgarini, V. Zwiller, and M. E. Reimer, Ultraclean emission from InAsP quantum dots in defect-free wurtzite InP nanowires, Nano Lett. **12**, 5919 (2012).

[28] M. Bouwes Bavinck, M. Zieliński, B. J. Witek, T. Zehender, E. P. A. M. Bakkers, and V. Zwiller, Controlling a nanowire quantum dot band gap using a straining dielectric envelope, Nano Lett. **12**, 6206 (2012).

[29] S. Yanase, H. Sasakura, S. Hara, and J. Motohisa, Single-photon emission from InAsP quantum dots embedded in density-controlled inp nanowires, Jpn. J. Appl. Phys. **56**, 04CP04 (2017).

[30] K. Kowalik, O. Krebs, A. Lemaître, S. Laurent, P. Senellart, P. Voisin, and J. A. Gaj, Influence of an in-plane electric field on exciton fine structure in InAs-GaAs self-assembled quantum dots, Appl. Phys. Lett. **86**, 041907 (2005).

[31] A. J. Bennett, M. A. Pooley, R. M. Stevenson, M. B. Ward, R. B. Patel, A. B. de La Giroday, N. Sköld, I. Farrer, C. A. Nicoll, D. A. Ritchie, and A. J. Shields, Electric-field-induced coherent coupling of the exciton states in a single quantum dot, Nat. Phys. **6**, 947 (2010).

[32] R. M. Stevenson, R. J. Young, P. See, D. G. Gevaux, K. Cooper, P. Atkinson, I. Farrer, D. A. Ritchie, and A. J. Shields, Magnetic-field-induced reduction of the exciton polarization splitting in InAs quantum dots, Phys. Rev. B **73**, 033306 (2006).

[33] B. D. Gerardot, S. Seidl, P. A. Dalgarno, R. J. Warburton, D. Granados, J. M. Garcia, K. Kowalik, O. Krebs, K. Karrai, A. Badolato, and P. M. Petroff, Manipulating exciton fine structure in quantum dots with a lateral electric field, Appl. Phys. Lett. **90**, 041101 (2007).

[34] S. Seidl, M. Kroner, A. Högele, K. Karrai, R. J. Warburton, A. Badolato, and P. M. Petroff, Effect of uniaxial stress on excitons in a self-assembled quantum dot, Appl. Phys. Lett. **88**, 203113 (2006).

[35] J. D. Plumhof, V. Křápek, F. Ding, K. D. Jöns, R. Hafenbrak, P. Klenovský, A. Herklotz, K. Dörr, P. Michler, A. Rastelli, and O. G. Schmidt, Strain-induced anticrossing of bright exciton levels in single self-assembled GaAs/$Al_xGa_{1-x}As$ and $In_xGa_{1-x}As$/GaAs quantum dots, Phys. Rev. B **83**, 121302(R) (2011).

[36] F. Ding, R. Singh, J. D. Plumhof, T. Zander, V. Křápek, Y. H. Chen, M. Benyoucef, V. Zwiller, K. Dörr, G. Bester,

A. Rastelli, and O. G. Schmidt, Tuning the Exciton Binding Energies in Single Self-Assembled InGaAs/GaAs Quantum Dots by Piezoelectric-Induced Biaxial Stress, Phys. Rev. Lett. **104**, 067405 (2010).

[37] J. Wang, M. Gong, G.-C. Guo, and L. He, Eliminating the fine structure splitting of excitons in self-assembled InAs/GaAs quantum dots via combined stresses, Appl. Phys. Lett. **101**, 063114 (2012).

[38] R. Trotta, E. Zallo, C. Ortix, P. Atkinson, J. D. Plumhof, J. van den Brink, A. Rastelli, and O. G. Schmidt, Universal Recovery of the Energy-Level Degeneracy of Bright Excitons in InGaAs Quantum Dots without a Structure Symmetry, Phys. Rev. Lett. **109**, 147401 (2012).

[39] R. Trotta, J. S. Wildmann, E. Zallo, O. G. Schmidt, and A. Rastelli, Highly entangled photons from hybrid piezoelectric-semiconductor quantum dot devices, Nano lett. **14**, 3439 (2014).

[40] S. Tomić and N. Vukmirović, Symmetry reduction in multi-band Hamiltonians for semiconductor quantum dots: The role of interfaces and higher energy bands, J. Appl. Phys. **110**, 053710 (2011).

[41] O. Marquardt, S. Schulz, C. Freysoldt, S. Boeck, T. Hickel, E. P. O'Reilly, and J. Neugebauer, A flexible, plane-wave based multiband $\mathbf{k}\cdot\mathbf{p}$ model, Opt. Quantum Electron. **44**, 183 (2011).

[42] R. Singh and G. Bester, Effects of atomic ordering on the electronic and optical properties of self-assembled $In_xGa_{1-x}As/GaAs$ semiconductor quantum dots, Phys. Rev. B **84**, 241402(R) (2011).

[43] G. W. Bryant, N. Malkova, and J. Sims, Mechanism for controlling the exciton fine structure in quantum dots using electric fields: Manipulation of exciton orientation and exchange splitting at the atomic scale, Phys. Rev. B **88**, 161301(R) (2013).

[44] M. Zieliński, Valence band offset, strain and shape effects on confined states in self-assembled InAs/InP and InAs/GaAs quantum dots, J. Phys.: Condens. Matter **25**, 465301 (2013).

[45] M. Korkusinski and P. Hawrylak, Atomistic theory of emission from dark excitons in self-assembled quantum dots, Phys. Rev. B **87**, 115310 (2013).

[46] P. N. Keating, Effect of invariance requirements on the elastic strain energy of crystals with application to the diamond structure, Phys. Rev. **145**, 637 (1966).

[47] R. M. Martin, Elastic properties of ZnS structure semiconductors, Phys. Rev. B **1**, 4005 (1970).

[48] W. Jaskólski, M. Zieliński, G. W. Bryant, and J. Aizpurua, Strain effects on the electronic structure of strongly coupled self-assembled InAs/GaAs quantum dots: Tight-binding approach, Phys. Rev. B **74**, 195339 (2006).

[49] T. Saito and Y. Arakawa, Electronic structure of piezoelectric $In_{0.2}Ga_{0.8}N$ quantum dots in gan calculated using a tight-binding method, Physica E **15**, 169 (2002).

[50] G. Bester, X. Wu, D. Vanderbilt, and A. Zunger, Importance of Second-Order Piezoelectric Effects in Zinc-Blende Semiconductors, Phys. Rev. Lett. **96**, 187602 (2006).

[51] G. Bester, A. Zunger, X. Wu, and D. Vanderbilt, Effects of linear and nonlinear piezoelectricity on the electronic properties of InAs/GaAs quantum dots, Phys. Rev. B **74**, 081305(R) (2006).

[52] A. Beya-Wakata, P.-Y. Prodhomme, and G. Bester, First- and second-order piezoelectricity in III-V semiconductors, Phys. Rev. B **84**, 195207 (2011).

[53] G. Tse, J. Pal, U. Monteverde, R. Garg, V. Haxha, M. Migliorato, and S. Tomić, Non-linear piezoelectricity in zinc blende GaAs and InAs semiconductors, J. Appl. Phys. **114**, 073515 (2013).

[54] M. A. Caro, S. Schulz, and E. P. O'Reilly, Origin of nonlinear piezoelectricity in III-V semiconductors: Internal strain and bond ionicity from hybrid-functional density functional theory, Phys. Rev. B **91**, 075203 (2015).

[55] J.-M. Jancu, R. Scholz, F. Beltram, and F. Bassani, Empirical $spds^*$ tight-binding calculation for cubic semiconductors: General method and material parameters, Phys. Rev. B **57**, 6493 (1998).

[56] D. J. Chadi, Spin-orbit splitting in crystalline and compositionally disordered semiconductors, Phys. Rev. B **16**, 790 (1977).

[57] M. Zieliński, Including strain in atomistic tight-binding Hamiltonians: An application to self-assembled InAs/GaAs and InAs/InP quantum dots, Phys. Rev. B **86**, 115424 (2012).

[58] S. Lee, F. Oyafuso, P. von Allmen, and G. Klimeck, Boundary conditions for the electronic structure of finite-extent embedded semiconductor nanostructures, Phys. Rev. B **69**, 045316 (2004).

[59] M. Zieliński, Multi-scale simulations of semiconductor nanostructures, Acta Phys. Pol. A **122**, 312 (2012).

[60] M. Zieliński, M. Korkusinski, and P. Hawrylak, Atomistic tight-binding theory of multiexciton complexes in a self-assembled InAs quantum dot, Phys. Rev. B **81**, 085301 (2010).

[61] M. Świderski and M. Zieliński, Atomistic theory of excitonic fine structure in InAs/InP nanowire quantum dot molecules, Phys. Rev. B **95**, 125407 (2017).

[62] X. Ma, G. W. Bryant, and M. F. Doty, Hole spins in an InAs/GaAs quantum dot molecule subject to lateral electric fields, Phys. Rev. B **93**, 245402 (2016).

[63] *Single Quantum Dots: Fundamentals, Applications and New Concepts*, edited by P. Michler, *Topics in Applied Physics*, Vol. 90 (Springer, New York, 2003).

[64] S. Lee, L. Jönsson, J. W. Wilkins, G. W. Bryant, and G. Klimeck, Electron-hole correlations in semiconductor quantum dots with tight-binding wave functions, Phys. Rev. B **63**, 195318 (2001).

[65] S. Schulz, S. Schumacher, and G. Czycholl, Tight-binding model for semiconductor quantum dots with a wurtzite crystal structure: From one-particle properties to Coulomb correlations and optical spectra, Phys. Rev. B **73**, 245327 (2006).

[66] P. T. Różański and M. Zieliński, Linear scaling approach for atomistic calculation of excitonic properties of 10-million-atom nanostructures, Phys. Rev. B **94**, 045440 (2016).

[67] P. T. Różański and M. Zieliński, Efficient computation of Coulomb and exchange integrals for multi-million atom nanostructures, Comput. Phys. Commun. **238**, 254 (2019).

[68] A. Y. Egorov, A. E. Zhukov, P. S. Kop'ev, N. N. Ledentsov, M. V. Maksimov, and V. M. Ustinov, Effect of deposition conditions on the formation of (In,Ga)As quantum clusters in a GaAs matrix, Semiconductors **28**, 809 (1994).

[69] I. Kegel, T. H. Metzger, A. Lorke, J. Peisl, J. Stangl, G. Bauer, K. Nordlund, W. V. Schoenfeld, and P. M. Petroff, Determination of strain fields and composition of self-organized quantum dots using x-ray diffraction, Phys. Rev. B **63**, 035318 (2001).

[70] N. Liu, J. Tersoff, O. Baklenov, A. L. Holmes, and C. K. Shih, Nonuniform Composition Profile in $In_{0.5}Ga_{0.5}As$ alloy quantum dots, Phys. Rev. Lett. **84**, 334 (2000).

[71] A. Lemaître, G. Patriarche, and F. Glas, Composition profiling of InAs/Ga as quantum dots, Appl. Phys. Lett. **85**, 3717 (2004).

[72] C. Dion, P. Desjardins, N. Shtinkov, M. D. Robertson, F. Schiettekatte, P. J. Poole, and S. Raymond, Intermixing during growth of InAs self-assembled quantum dots in InP: A photoluminescence and tight-binding investigation, Phys. Rev. B **77**, 075338 (2008).

[73] W. Sheng and S. J. Xu, Optical characterization of structure for semiconductor quantum dots, Phys. Rev. B **77**, 113305 (2008).

[74] T. Warming, E. Siebert, A. Schliwa, E. Stock, R. Zimmermann, and D. Bimberg, Hole-hole and electron-hole exchange interactions in single InAs/GaAs quantum dots, Phys. Rev. B **79**, 125316 (2009).

[75] A. J. Williamson, L. W. Wang, and A. Zunger, Theoretical interpretation of the experimental electronic structure of lens-shaped self-assembled InAs/GaAs quantum dots, Phys. Rev. B **62**, 12963 (2000).

[76] W.-d. Sheng, M. Korkusinski, A. D. Güçlü, M. Zielinski, P. Potasz, E. S. Kadantsev, O. Voznyy, and P. Hawrylak, Electronic and optical properties of semiconductor and graphene quantum dots, Front. Phys. **7**, 328 (2012).

[77] P. W. Fry, I. E. Itskevich, D. J. Mowbray, M. S. Skolnick, J. J. Finley, J. A. Barker, E. P. O'Reilly, L. R. Wilson, I. A. Larkin, P. A. Maksym, M. Hopkinson, M. Al-Khafaji, J. P. R. David, A. G. Cullis, G. Hill, and J. C. Clark, Inverted Electron-Hole Alignment in InAs-GaAs Self-Assembled Quantum Dots, Phys. Rev. Lett. **84**, 733 (2000).

[78] J. A. Barker and E. P. O'Reilly, Theoretical analysis of electron-hole alignment in InAs-GaAs quantum dots, Phys. Rev. B **61**, 13840 (2000).

[79] A. Schliwa, M. Winkelnkemper, and D. Bimberg, Impact of size, shape, and composition on piezoelectric effects and electronic properties of In(Ga)As/GaAs quantum dots, Phys. Rev. B **76**, 205324 (2007).

[80] M. Zieliński, From quantum dots to quantum dashes: Excitonic spectra of highly elongated InAs/InP nanostructures, Phys. Rev. B **99**, 205402 (2019).

[81] T. Takagahara, Theory of exciton doublet structures and polarization relaxation in single quantum dots, Phys. Rev. B **62**, 16840 (2000).

[82] E. Kadantsev and P. Hawrylak, Theory of exciton fine structure in semiconductor quantum dots: Quantum dot anisotropy and lateral electric field, Phys. Rev. B **81**, 045311 (2010).

[83] E. L. Ivchenko, *Optical Spectroscopy of Semiconductor Nanostructures*, 2nd ed. (Alpha Science, Oxford, 2005).

[84] J.-W. Luo and A. Zunger, Geometry of epitaxial GaAs/(Al,Ga)As quantum dots as seen by excitonic spectroscopy, Phys. Rev. B **84**, 235317 (2011).

[85] E. Tsitsishvili, Impact of heavy hole–light hole coupling on the exciton fine structure in quantum dots, Physica E **87**, 161 (2017).

[86] T. Smoleński, T. Kazimierczuk, M. Goryca, T. Jakubczyk, Ł. Kłopotowski, Ł. Cywński, P. Wojnar, A. Golnik, and P. Kossacki, In-plane radiative recombination channel of a dark exciton in self-assembled quantum dots, Phys. Rev. B **86**, 241305(R) (2012).

[87] C. Tonin, R. Hostein, V. Voliotis, R. Grousson, A. Lemaitre, and A. Martinez, Polarization properties of excitonic qubits in single self-assembled quantum dots, Phys. Rev. B **85**, 155303 (2012).

[88] Y. Léger, L. Besombes, L. Maingault, and H. Mariette, Valence-band mixing in neutral, charged, and Mn-doped self-assembled quantum dots, Phys. Rev. B **76**, 045331 (2007).

[89] M. Gawełczyk, M. Syperek, A. Maryński, P. Mrowiński, L. Dusanowski, K. Gawarecki, J. Misiewicz, A. Somers, J. P. Reithmaier, S. Höfling, and G. Sęk, Exciton lifetime and emission polarization dispersion in strongly in-plane asymmetric nanostructures, Phys. Rev. B **96**, 245425 (2017).

[90] M. Zieliński, Vanishing fine structure splitting in highly asymmetric InAs/InP quantum dots without wetting layer, Sci. Rep. **10**, 13542 (2020).

[91] C. Pryor, J. Kim, L. W. Wang, A. J. Williamson, and A. Zunger, Comparison of two methods for describing the strain profiles in quantum dots, J. Appl. Phys. **83**, 2548 (1998).

[92] C. G. Van de Walle, Band lineups and deformation potentials in the model-solid theory, Phys. Rev. B **39**, 1871 (1989).

[93] S.-H. Wei and A. Zunger, Optical properties of zinc-blende semiconductor alloys: Effects of epitaxial strain and atomic ordering, Phys. Rev. B **49**, 14337 (1994).

[94] G. Klimeck, F. Oyafuso, T. B. Boykin, R. C. Bowen, and P. von Allmen, Development of a nanoelectronic 3-D (NEMO 3-D) simulator for multimillion atom simulations and its application to alloyed quantum dots, CMES **3**, 601 (2002).

[95] A. Zunger, Pseudopotential theory of semiconductor quantum dots, Physica Status Solidi B **224**, 727 (2001).

[96] V. Mlinar, M. Bozkurt, J. M. Ulloa, M. Ediger, G. Bester, A. Badolato, P. M. Koenraad, R. J. Warburton, and A. Zunger, Structure of quantum dots as seen by excitonic spectroscopy versus structural characterization: Using theory to close the loop, Phys. Rev. B **80**, 165425 (2009).

[97] N. Sköld, A. B. de la Giroday, A. J. Bennett, I. Farrer, D. A. Ritchie, and A. J. Shields, Electrical Control of the Exciton Fine Structure of a Quantum Dot Molecule, Phys. Rev. Lett. **110**, 016804 (2013).

[98] J. G. Díaz, G. W. Bryant, W. Jaskólski, and M. Zieliński, Theory of InP nanocrystals under pressure, Phys. Rev. B **75**, 245433 (2007).

[99] M. Świderski and M. Zieliński, Electric field tuning of excitonic fine-structure splitting in asymmetric InAs/InP nanowire quantum dot molecules, Phys. Rev. B **100**, 235417 (2019).

[100] J. Pérez-Conde and A. K. Bhattacharjee, Exciton states and optical properties of CdSe nanocrystals, Phys. Rev. B **63**, 245318 (2001).

[101] S. Lee, J. Kim, L. Jönsson, J. W. Wilkins, G. W. Bryant, and G. Klimeck, Many-body levels of optically excited and multiply charged InAs nanocrystals modeled by semiempirical tight binding, Phys. Rev. B **66**, 235307 (2002).

[102] T. B. Boykin and P. Vogl, Dielectric response of molecules in empirical tight-binding theory, Phys. Rev. B **65**, 035202 (2001).

[103] K. Leung and K. B. Whaley, Electron-hole interactions in silicon nanocrystals, Phys. Rev. B **56**, 7455 (1997).

[104] M. Świderski and M. Zieliński, Exact diagonalization approach for atomistic calculation of piezoelectric effects in semiconductor quantum dots, Acta Phys. Pol. A **129**, A-79 (2016).